

Soft X-Ray Excess from Shocked Accreting Plasma in Active Galactic Nuclei

KEIGO FUKUMURA^{1,2,3}, DOUGLAS HENDRY¹, PETER CLARK¹, FRANCESCO TOMBESI^{4,5},
AND MASAOKI TAKAHASHI⁶

July 9, 2021

Received _____; accepted _____

¹Department of Physics and Astronomy, James Madison University, Harrisonburg, VA 22807

²Email: fukumukx@jmu.edu

³KITP Scholar at UC Santa Barbara

⁴Astrophysics Science Division, NASA/Goddard Space Flight Center, Greenbelt, MD 20771

⁵Department of Astronomy and CRESST, University of Maryland, College Park, MD20742

⁶Department of Physics and Astronomy, Aichi University of Education, Kariya, Aichi 448-8542, Japan

ABSTRACT

We propose a novel theoretical model to describe a physical identity of the soft X-ray excess, ubiquitously detected in many Seyfert galaxies, by considering a steady-state, axisymmetric plasma accretion within the innermost stable circular orbit (ISCO) around a black hole (BH) accretion disk. We extend our earlier theoretical investigations on general relativistic magnetohydrodynamic (GRMHD) accretion which has implied that the accreting plasma can develop into a standing shock for suitable physical conditions causing the downstream flow to be sufficiently hot due to shock compression. We numerically calculate to examine, for sets of fiducial plasma parameters, a physical nature of fast MHD shocks under strong gravity for different BH spins. We show that thermal seed photons from the standard accretion disk can be effectively Compton up-scattered by the energized sub-relativistic electrons in the hot downstream plasma to produce the soft excess feature in X-rays. As a case study, we construct a three-parameter Comptonization model of inclination angle θ_{obs} , disk photon temperature kT_{in} and downstream electron energy kT_e to calculate the predicted spectra in comparison with a 60 ks *XMM-Newton*/EPIC-pn spectrum of a typical radio-quiet Seyfert 1 AGN, Ark 120. Our χ^2 -analyses demonstrate that the model is plausible in successfully describing data for both non-spinning and spinning BHs with the derived range of $61.3 \text{ keV} \lesssim kT_e \lesssim 144.3 \text{ keV}$, $21.6 \text{ eV} \lesssim kT_{\text{in}} \lesssim 34.0 \text{ eV}$ and $17.5^\circ \lesssim \theta_{\text{obs}} \lesssim 42.6^\circ$ indicating a compact Comptonizing region of 3 – 4 gravitational radii that resembles the putative X-ray coronae.

Subject headings: accretion, accretion disks — galaxies: Seyfert — methods: numerical — galaxies: individual (Ark 120) — (magnetohydrodynamics:) MHD

1. Introduction

A broad-band synergistic study of active galactic nuclei (AGNs) in recent years has revealed a number of underlying spectroscopic components that is critical to understand a fundamental physical process around central engines of AGNs. Especially in a close proximity to a nucleus well within the sphere of influence by a supermassive black hole (BH), state-of-the-art X-ray spectroscopies today have clearly demonstrated a complexity of AGN physics associated with inflows as well as outflows. Among others is a “soft X-ray excess” which is an excessive amount of spectral feature below ~ 2 keV above a baseline continuum extrapolated from a hard X-ray range (typically from a 2 – 10 keV power-law component of photon index $\Gamma \sim 2$), and it is known to be present among Seyfert galaxies particularly in the so called the narrow-line Seyfert 1 (NLS1) AGNs — a sub-class of the type 1 Seyfert galaxies of certain spectroscopic properties. Since its first extensive analysis as a part of the multi-wavelength campaign (EUV and soft/hard X-ray with *ROSAT*) of NLS1s about two decades ago (e.g. Osterbrock & Pogge 1985; Goodrich 1989; Walter & Fink 1993; Boller et al. 1996; Leighly 1999a,b), only a small pieces of observational facts have been obtained even from more recent observations about the origin of soft excess; (1) Its presence is almost ubiquitous in NLS1 galaxies of both smaller and larger BH masses. (2) Its equivalent blackbody temperature appears to be almost universally $\sim 0.1 - 0.2$ keV regardless of the objects. (3) Its output power occupies a good fraction of a total AGN luminosity (Boller et al. 1996). In the context of the standard accretion disk (Shakura & Sunyaev 1973) its maximum effective temperature is well-defined to be only $kT \sim 10(\dot{m}/M_8)^{1/4}$ eV where $\dot{m} \equiv \dot{M}/\dot{M}_{\text{Edd}}$ is the AGN mass-accretion rate normalized by the Eddington mass-accretion rate for a BH mass M with $M_8 \equiv M/(10^8 M_\odot)$. Not only is it challenging to account for the observed nearly-constant “temperature” of the soft excess by the standard disk model (e.g. Shakura & Sunyaev 1973), the model, even with an extreme assumption of high accretion rate and low-mass BH, could barely bring the peak of disk spectrum only up to $kT \lesssim 0.1$ keV, which means that the standard disk emission should make virtually no significant contribution to the observed soft excess (e.g. Laor et al. 1997) thus fails to explain its physical origin¹. While long sought, the nature of this spectral component is quite elusive so far.

A number of plausible scenarios to explain the physics of the soft excess, among others, includes (1) a continuum component strongly absorbed by a series of ionized absorbers in a relativistic outflow whose spectral curvature could then be interpreted as a falsified “excess” feature (Schurch & Done 2006, 2008; Gierliński & Done 2004; Middleton et al. 2007), (2) ionized atomic processes from an inner part of the disk illuminated via light bending

¹On the other hand, a slim disk configuration - another regime of accretion disks - has been also studied for NLS1s (e.g. Mineshige et al. 2000).

(e.g. Miniutti & Fabian 2004; Fabian et al. 2004; Kara et al. 2015) to produce a series of relativistically-blurred emission lines to mimic an apparently smooth “excess” spectral shape (e.g. Ross & Fabian 2005; Crummy et al. 2006; Fabian et al. 2009; Ponti et al. 2010; Nardini et al. 2011; De Marco et al. 2013) with a predicted correlation between the hard and soft X-rays (e.g. Vasudevan et al. 2014, Boissay et al. 2015 in prep) and (3) a Comptonization of the disk photons by some means such as corona ($kT = 1$ keV) or upper layer of the disk (e.g. Petrucci et al. 2004; Mehdipour et al. 2011; Done et al. 2012; Zhong & Wang 2013; Noda et al. 2013; Di Gesu et al. 2014) with an expectation of a correlation between UV and soft X-ray flux (Mehdipour et al. 2011). In particular, Petrucci et al. (2013), for example, has made a synergistic spectral analysis (from UV to hard X-ray) based on the multiwavelength campaign on a bright Seyfert galaxy, Mrk 509, focusing in part on the observed soft excess. Motivated by the implied correlation between UV and soft X-ray flux from *XMM-Newton* and INTEGRAL observations, the authors proposed a thermal Comptonization model to describe the physical origin of both soft excess and power-law components.

On the other hand, accretion physics has been extensively studied for decades particularly from theoretical aspects including semi-analytic investigations as well as global numerical simulations in an effort to further understand its physical nature and observational consequences. Many of these works on BH accretion in general have broadly revealed, among others, an important generic feature of accretion; i.e. the formation of shocks as accreting plasma is subject to outward forces via a number of decelerating mechanisms (e.g. , Abramowicz & Prasanna (1990, MNRAS, 245, 720)) and develop a shock front at $r = r_{\text{sh}}$ within the radius of the inner edge of a magnetized accretion disk², perhaps equivalent to a stable circular orbit (ISCO) for a pure HD Keplerian disk, before crossing an event horizon at $r = r_H$. Previous studies include hydrodynamic shocks (e.g. Nobuta & Hanawa 1994; Lu et al. 1997; Chakrabarti 1990; Fukumura et al. 2004) and magnetohydrodynamic (MHD) shocks (e.g., Koide et al. 1998, 2000; Das & Chakrabarti 2007; Takahashi et al. 2002, hereafter T02; Takahashi et al. 2006, hereafter T06; Fukumura et al. 2007, hereafter F07; Fukumura & Kazanas 2007b; Takahashi & Takahashi 2010). In particular, an extensive theoretical studies of various types of shocks have been conducted to date in an attempt to understand its dynamical behavior; e.g. shock oscillation in the context of quasi-periodic oscillations (QPOs) and its spectroscopic signatures (e.g. Chakrabarti & Titarchuk 1995; Molteni et al. 1996, 1999; Acharya et al. 2002; Okuda et al. 2004, 2007; Nagakura & Yamada 2008) that may be relevant for XRBs, for example. Independent GRMHD simulations of the tilted accretion

²Armitage et al. (2001) has found an ISCO-like edge in their pseudo-Newtonian MHD accretion simulations.

disk clearly show that the compression of the plunging plasma in the inner region ($r \lesssim 10r_g$) leads to the formation of standing shocks (e.g. Fragile et al. 2007; Fragile & Blaes 2008; Generozov et al. 2014) depending on the characteristics of the disk geometry and the BH spin (e.g. Morales et al. 2014). The expected highly magnetized shocked region may perhaps correspond to the magnetically-arrested plasma seen in the other large-scale simulations (e.g. Tchekhovskoy et al. 2011).

As a generic feature of accretion shocks unambiguously revealed in the earlier theoretical work by many authors, the downstream flow across the shock front is thus compressed and heated up efficiently to generate additional entropy all the way down to the horizon unless a cooling process is sufficiently efficient (e.g. Chakrabarti 1995; Chakrabarti & Titarchuk 1995). While the detailed formalism and numerical methodology in these works are different, the presence of shocks in accretion is strongly favored in these calculations. As a result, the postshock region at small radii will provide an ideal site where the accelerated electrons could Compton up-scatter the thermal photons from an accretion disk. This process can produce a characteristic excess component in soft X-ray band below $\sim 1 - 2$ keV as a substantially modified disk blackbody radiation, and its spectral shape depends on a number of variables related to MHD accretion processes. Our current work is thus motivated by this long-standing implication of shock formation in accretion.

Utilizing the models of T02 and F07, we thus make a preliminary attempt in this paper to calculate the expected soft X-ray excess spectrum in the context of the well-explored GRMHD shocked accretion models in the past work (T02, F07). As depicted in Figure 1, we assume magnetized equatorial accretion with its inner edge of r_{in} (similar to the standard Shakura-Sunyaev disk Shakura & Sunyaev 1973) in this model as a reservoir for incoming EUV photons. Plasma near $r = r_{\text{in}}$ (i.e. ISCO-like boundary radius as discussed in Armitage et al. 2001) eventually begins to plunge in and subsequently develops an adiabatic standing shock at a very small radius determined primarily by the plasma conditions such as energy, angular momentum and mass-accretion rate, for example. It is reminded, in the case of GRMHD accretion, that there exist a multiple magnetosonic points between r_{in} and r_H (see T02 and T06 for more detailed discussion). The downstream region is therefore heated by adiabatic shock compression creating a centrally-concentrated, compact hot region similar to the putative X-ray coronae (e.g. Fabian et al. 2015; Wilkins et al. 2015). The incoming blueshifted disk photons towards the downstream plasma is then Comptonized by hot electrons in the postshock flow producing the soft excess. Note, however, that the proposed Comptonization in our model is attributed exclusively to accelerated electrons in the rest-frame of downstream plasma accretion independent of the bulk motion of the flow (e.g., see, Titarchuk et al. 1996, for a fundamental difference from the standard bulk motion Comptonization model). Our study focuses on explicitly constraining the defining parameters of the GRMHD accretion models by clearly identifying the physical origin of the observed soft excess feature as a shock-heating innermost downstream flow. Our ultimate

goal is to systematically understand the physics of the observed soft excess component in a coherent scenario by applying the model to a large sample of relevant Seyfert AGNs. As an example in this paper, we have analyzed a stereotypical radio-quiet Seyfert AGN, Ark 120, as an application of the model and demonstrate its viability via χ^2 -statistics.

We will briefly review the characteristics of the GRMHD accretion in §2 by presenting fiducial shocked accretion solutions. Then, our methodology for calculating the Comptonized spectrum for a series of solutions in Kerr geometry is discussed in §.3 with GR effects being fully implemented. In §4 we show our preliminary results for a 60-ks *XMM-Newton*/EPIC-pn spectrum of Ark 120 as a case study successfully constraining primary variables in the model. We summarize and discuss the implications of the model in §5.

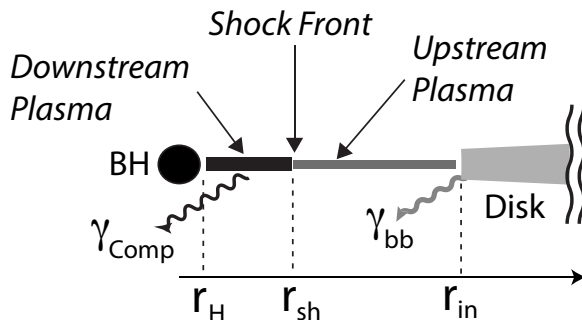


Fig. 1.— A schematic diagram illustrating nonthermal Comptonizing process of thermal disk photons of energy kT_{in} (labeled as γ_{bb}) by downstream energetic electrons of energy kT_e to produce the Comptonized photons (labeled as γ_{Comp}). See texts for the radii labelled.

2. GRMHD Models with Shocked Accreting Plasma

2.1. Formalism

We adopt the well-defined model for GRMHD shock formation in accreting plasma discussed in a series of papers (T02, T06, F07) in a formalism closely aligned with other simulations, for example, by Pu et al. (2015). We consider stationary ($\partial_t = 0$) and axisymmetric ($\partial_\phi = 0$) ideal MHD accretion in Kerr geometry whose spacetime metric components $g_{\mu\nu}$ is described by the Boyer-Lindquist coordinates (t, r, θ, ϕ)

$$ds^2 = \left(1 - \frac{2Mr}{\Sigma}\right) dt^2 + \frac{4Mar \sin^2 \theta}{\Sigma} dt d\phi - \frac{A \sin^2 \theta}{\Sigma} d\phi^2 - \frac{\Sigma}{\Delta} dr^2 - \Sigma d\theta^2, \quad (1)$$

with the conventional (+ – – –) metric signature where M is BH mass and a is its angular momentum per BH mass (i.e. spin parameter) with $\Delta \equiv r^2 - 2Mr + a^2$, $\Sigma \equiv r^2 + a^2 \cos^2 \theta$, and $A \equiv (r^2 + a^2)^2 - a^2 \Delta \sin^2 \theta$. The length scale in this paper is normalized to the gravitational radius r_g where $r_g \equiv GM/c^2$ with G and c being the gravitational constant and speed of light, respectively.

In the context of ideal GRMHD, the property of accreting plasma is governed by (1) particle number conservation law: $(nu^\alpha)_{;\alpha}$ where n is the proper particle number density and u^α is the plasma four-velocity, (2) equation of motion: $T^{\alpha\beta}_{;\beta} = 0$ where $T^{\alpha\beta}$ is the energy-momentum tensor for magnetized plasmas and (3) ideal MHD condition: $u^\beta F_{\alpha\beta} = 0$ where $F_{\alpha\beta}$ is the electromagnetic field tensor. The poloidal plasma four-velocity is given as $u_p^2 \equiv -u^\alpha u_\alpha$. The energy-momentum tensor $T^{\alpha\beta}$ is given by

$$T^{\alpha\beta} \equiv n\mu u^\alpha u^\beta - P g^{\alpha\beta} + \frac{1}{4\pi} \left(F^{\alpha\gamma} F^\beta_\gamma + \frac{1}{4} g^{\alpha\beta} F^2 \right), \quad (2)$$

where $F^2 \equiv F_{\mu\nu} F^{\mu\nu}$ and $\mu = (\rho + P)/n$ is the relativistic enthalpy, P is the thermal gas pressure, ρ is the total energy density and n the plasma number density. Note that we assume the polytropic relation as $P = K \rho_o^{\Gamma_p}$ where K is related to entropy of the plasma with the polytropic index Γ_p and $\rho_o = nm_e$ is the rest-mass density with the particle rest-mass m_e .

Assuming a steady-state, axisymmetric plasma, one can describe a topology of magnetic field lines using the magnetic stream function $\Psi(r, \theta)$ which is constant along a given field line. The plasma is frozen-in and flows along the field lines with five constants of motion in this formalism; angular velocity of field lines $\Omega_F(\Psi)$, plasma flux to magnetic flux ratio $\eta(\Psi)$, total energy of accreting plasma $E(\Psi)$, total angular momentum of plasma $L(\Psi)$ and entropy $S(\Psi)$. The total energy and angular momentum of the adiabatic plasma are given by

$$E \equiv \mu u_t - \frac{\Omega_F B_\phi}{4\pi\eta}, \quad (3)$$

$$L \equiv -\mu u_\phi - \frac{B_\phi}{4\pi\eta}, \quad (4)$$

where $B_\phi = (\Delta/\Sigma)F_{\theta r} \sin \theta$ is the toroidal component of the magnetic field seen by a distant observer. From the poloidal components of the equation of motion with the above five constants, one can derive the general relativistic Bernoulli equation (aka. poloidal/wind equation) as

$$\mu^2(1 + u_p^2) = E^2 [(\alpha - 2M^2)f^2 - \delta], \quad (5)$$

where $u_p^2 \equiv -(u_\alpha u^\alpha) = -(u_r u^r + u_\theta u^\theta)$ is the poloidal plasma velocity with f, δ and α being the functions of metric components and conserved quantities (see T06 and F07). Here, M_A

is the relativistic Alfvén Mach number³ defined as

$$M_A^2 \equiv \frac{4\pi\mu n u_p^2}{B_p^2}, \quad (6)$$

where B_p is the poloidal magnetic field in the distant observer’s frame (e.g. T06; F07). Technically speaking, a field geometry should be self-consistently calculated by the force-balance equation in a direction parallel to the streamline described by the Grad-Shafranov (GS) equation in general relativistic regime. However, we will adopt a simplistic approach (e.g. T02; F07) and specify a purely conical field line geometry such that the poloidal magnetic field is given by $|\mathbf{B}_p| \propto (\Delta\Sigma)^{-1/2}$ following the split-monopole approximation (e.g. Michel 1973; Wald 1974; Blandford & Znajek 1977, ; see also §5). In this formalism, the field topology is thus parameterized to be conical. Plasma is assumed to be adiabatic of single temperature and we ignore its self-gravity and viscous nature.

To describe the plasma kinematics from an intuitive perspective, we calculate and express the three-velocity components of plasma in two different locally-flat inertial frames (e.g. Manmoto 2000); i.e. radial component v_{CRF}^r defined in a corotating reference frame (CRF) where a local observer is corotating with the plasma such that

$$v_{\text{CRF}}^r \equiv \left(\frac{-u_r u^r}{1 - u_r u^r} \right)^{1/2}, \quad (7)$$

and toroidal component v_{LNRF}^ϕ defined in a locally non-rotating reference frame (LNRF) where a zero-angular-momentum-observer (ZAMO) is corotating with a BH such that

$$v_{\text{LNRF}}^\phi \equiv \frac{A}{r^2 \Delta^{1/2}} (\Omega - \omega), \quad (8)$$

where $\Omega \equiv u^\phi/u^t$ is the angular velocity of plasma and the frame-dragging $\omega \equiv -g_{t\phi}/g_{\phi\phi}$ has been subtracted off in LNRF so one sees the intrinsic plasma rotation locally. Note that in these reference frames it is guaranteed to have $v_{\text{CRF}}^r \rightarrow 1$ and $v_{\text{LNRF}}^\phi \rightarrow 0$ as $r \rightarrow r_H$ by definition (see §2.2 for results). To characterize the magnetized nature of the plasma, we examine the magnetization parameter σ defined in LNRF as the ratio of the outward Poynting flux to the inward net mass-energy flux of the accreting plasma such that

$$\sigma \equiv \frac{B_\phi g_{\phi\phi} (\Omega_F - \omega)}{4\pi\eta\mu u^t \rho_w^2}, \quad (9)$$

³The Mach number M_A can decrease while plasma speeds up if magnetic field strength increases faster.

where $\rho_w^2 \equiv g_{t\phi}^2 - g_{tt}g_{\phi\phi}$. Thus, the sign of σ in general can change as B_ϕ may switch its direction due to the global field geometry (see T02 and F07 for details).

Assuming that accreting plasma is initially injected from a plasma source (most likely near the inner edge of a magnetized accretion disk; see Fig. 1) with its toroidal velocity being predominant (i.e. $v_{\text{CRF}}^r < v_{\text{LNR}}^\phi$) onto a BH, physical plasma accretion must be trans-magnetosonic before reaching the event horizon going through two magnetosonic points (i.e. slow and fast magnetosonic points) and the Alfvén point. On the course of accretion, furthermore, accreting plasma is subject to various “obstacles” to slow down inwards; e.g. gas pressure, radiation pressure, magnetic force, and centrifugal barrier, for example. Via nonlinear processes, flow can develop into a shock front at some radius determined by a certain physical condition. Considering a proper jump condition across the shock front, one can determine a physically valid shock location r_{sh} . Note that both upstream and downstream plasma must be trans-magnetosonic on its own; i.e. the former (latter) must pass through the *outer (inner)* magnetosonic points and the Alfvén point. To simplify the problem we set the surface of a shock front to be normal to the magnetic field lines as in the previous calculations (e.g., T02, F07). Among different types of shocks, we consider here adiabatic (i.e. Rankine-Hugoniot) perpendicular shock conditions where cooling processes are so inefficient at the shock front that no energy (and angular momentum) is dissipated away. The condition can be analytically simplified as

$$\frac{1}{\Delta\Sigma} \left(\frac{M_1}{4\pi\eta} \right)^2 + \frac{\mu_1 - 1}{1 + N} \frac{\mu_1}{M_1^2} + \frac{(Ef_1)^2}{2} = \frac{1}{\Delta\Sigma} \left(\frac{M_2}{4\pi\eta} \right)^2 + \frac{\mu_2 - 1}{1 + N} \frac{\mu_2}{M_2^2} + \frac{(Ef_2)^2}{2}, \quad (10)$$

where the roots ($r = r_{\text{sh}}$) to this equation are “shock locations” and the subscripts “1” and “2” respectively denote upstream and downstream quantities. We have used $1 + N \equiv \Gamma_p/(\Gamma_p - 1)$. We will numerically calculate this radius across which particle number, energy, angular momentum, and magnetic flux are all simultaneously conserved (while density, temperature and velocity are discontinuous). Note that the enthalpy μ remains conserved due to adiabatic assumption but increases across the shock because of entropy generation. The local shock compression in the Newtonian view is then given by the velocity ratio as

$$\frac{n_2}{n_1} \equiv \frac{u_1^r}{u_2^r} = \frac{\mu_2 M_{A,1}^2}{\mu_1 M_{A,2}^2}. \quad (11)$$

As in the past work (e.g. T02; F07) we simply treat the shock front as a mathematical discontinuity rather than considering its actual finite internal structure (see, e.g., Le & Becker 2005; Becker et al. 2011, for considering particle transport at a diffusive shock front). It is reminded that the postshock downstream flow is heated across the shock front in the absence of efficient cooling mechanisms and remain hot under adiabatic flow assumption in this work.

Most importantly in the present work, we also introduce normalized electron thermal energy Θ_e to assess energetics of accelerated electrons in the heated downstream plasma due to shock compression as a function of radius as

$$\Theta_e(r) \equiv \frac{kT_e}{m_e c^2} = K \rho_o^{\Gamma_p - 1} = \frac{1}{1 + N} \left(\frac{\mu}{m_e c^2} - 1 \right), \quad (12)$$

where k is the Boltzman constant, $m_e c^2 = 511$ keV is the electron’s rest-mass energy and T_e is electron’s equivalent thermal temperature in a single-fluid approximation. Hence, the temperature is uniquely determined by plasma density and entropy which is closely related to plasma pressure as well from the polytropic assumption. Unlike the hot downstream flow, the upstream (preshock) plasma is assumed to have negligible thermal energy (i.e. $K \sim 0$) compared to its rest-mass energy in the cold flow limit (i.e. $\mu_1 \sim m_e c^2$ thus $\Theta_e \sim 0$ in the upstream region). In this limit, the slow magnetosonic point for the upstream plasma vanishes leaving only the Alfvén point and a fast magnetosonic point.

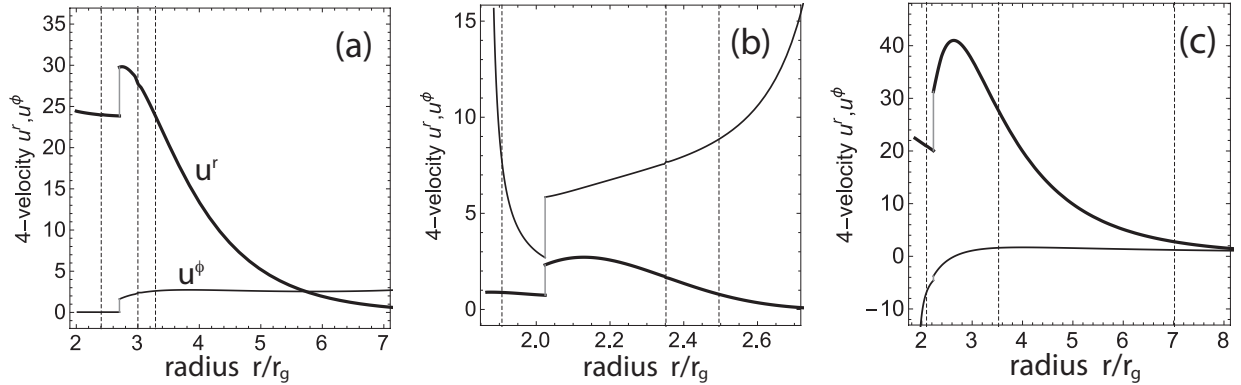


Fig. 2.— Radial profiles of four-velocity components u^r (thick solid) and u^ϕ (solid) for a fiducial accreting MHD plasma with (a) $a/M = 0$ (Schwarzschild BH), (b) 0.5 (prograde) and (c) -0.5 (retrograde). Vertical dotted lines denote the outer Alfvén radius (rightmost), outer fast-magnetosonic radius (middle) and the inner Alfvén radius (leftmost) as plasma accretes and develops a fast MHD shock as shown in vertical jump. See Table 1 for detailed model parameters.

Table 1. Characteristics of Fiducial GRMHD Plasma Accretion

| Conserved Parameter | Description | BH Spin a/M | | |
|-------------------------------|--------------------------------|---------------|---------|--------|
| | | -0.5 | 0 | 0.5 |
| E | Energy | 6.1 | 6.1 | 6.1 |
| L/E | Specific angular momentum | 2.1 | 2.3 | 3.96 |
| Ω_F | Angular velocity of field line | 0.02725 | 0.08334 | 0.2333 |
| $4\pi\eta$ | Scaled accretion energy | 0.0082 | 0.006 | 0.005 |
| r_A^{out}/r_g | Outer Alfvén radius | 7.01 | 3.28 | 2.82 |
| r_F^{out}/r_g | Outer fast radius | 3.52 | 3.01 | 2.49 |
| r_{sh}/r_g | Shock location | 2.23 | 2.70 | 1.99 |
| r_F^{in}/r_g | Inner fast radius | 2.09 | 2.41 | 1.90 |
| r_H/r_g | Event horizon | 1.86 | 2.0 | 1.86 |
| $\Theta_e(r = r_{\text{sh}})$ | Electron energy | 0.358 | 0.199 | 0.285 |

Note: Superscripts “in” and “out” respectively denote those radii for the “downstream” and “upstream” plasma.

2.2. Numerical Solutions for Shocked Plasma Accretion

Following the past work (T02, F07), we calculate a global property of physically valid plasma accretion for a given set of conservative quantities described in §2.1. Our calculations throughout this paper are restricted to the equatorial flows for simplicity (i.e. $\theta = \pi/2$ and $u^\theta = B^\theta = 0$) and we set the polytropic index $\Gamma_p = 4/3$ in the presence of the conical magnetic field. To exploit the parameter space as systematically as possible, a fiducial value of the plasma energy is chosen as $E = 6.1$ in all cases discussed here (see F07 for its relevance) along with the other conserved quantities and radii as listed in Table 1. Note that these characteristic radii are not free-parameters but determined by the shock conditions. We then vary the rest of the primary parameters, L/E and Ω_F for a given BH spin a and η in order to find the valid solutions (see T02 and F07 for a detailed numerical methodology).

As a representative solution for a given BH spin, normalized radial profiles of major characteristics of each shocked accretion is shown in Figures 2-4 for (a) $a/M = 0$, (b) 0.5 and (c) -0.5 along with its corresponding outer/inner fast-magnetosonic radii and the Alfvén radius (vertical dotted lines). A standing shock is denoted as a solid vertical line (gray) connecting upstream and downstream flows. Figure 2 shows the computed radial u^r and azimuthal u^ϕ components of the four-velocity in the Boyer-Lindquist coordinates. The plasma begins to plunge in near the ISCO along a magnetic field line radially accelerating by passing through the Alfvén point and the outer fast point. The upstream flow then forms a shock at $r = r_{\text{sh}}$ developing a hot downstream region followed by passing through the inner fast point before entering the event horizon in each BH spin case (a)-(c). Note that the upstream plasma starts slowing down due to a number of outward forces (e.g. Lorentz force and centrifugal barrier) just before forming a shock. In the case of a Schwarzschild BH in (a), the plasma motion becomes more and more radial towards the horizon (i.e. $u^r > u^\phi$). For a prograde BH in (b), the plasma starts to plunge in from the ISCO at smaller radius compared to (a) because the ISCO radius shifts more inward. Therefore, the plunging plasma acquires a larger toroidal velocity u^ϕ due to a faster Keplerian motion of the disk in the beginning. At small radius, the frame-dragging effect is prominent forcing the downstream flow to be corotating with the BH and u^ϕ dominates over u^r . On the other hand, around a retrograde BH in (c), the rotational sense of the upstream plasma ($u^\phi > 0$ at large radii) is eventually switched the other way around ($u^\phi < 0$ near the horizon) due to the frame-dragging, as expected. In other words, a distant observer in a flat spacetime sees the accreting plasma momentarily turn around at some point (i.e. $u^\phi = 0$) between the outer fast point and the shock location changing the direction of its toroidal motion.

A corresponding three-velocity of the plasma is calculated in a local reference frame of flat spacetime as shown in Figure 3. In all the cases the plasma is seen in CRF to radially approach the speed of light ($v_{\text{CRF}}^r \rightarrow 1$) in the course of accretion while toroidal motion

seen in LNRF eventually approach the spacetime rotational speed ($\Omega \rightarrow \omega$ thus $v_{\text{LNRF}}^\phi \rightarrow 0$) as expected. Note in (c) that the same “turn-around” behavior of the plasma toroidal motion is clearly seen in LNRF between the outer fast point and the shock location (i.e. $v_{\text{LNRF}}^\phi > 0 \rightarrow v_{\text{LNRF}}^\phi < 0$) due to the frame-dragging and in fact the plasma “overshoots” the ZAMO in LNRF until the shock occurs (thus v_{LNRF}^ϕ continues to increase in the same sense as the BH rotation). In the downstream flow, the shocked plasma stops “overshooting” the ZAMO eventually converging to the frame-dragging at the horizon as expected. It is counterintuitive to see in (c) that the plasma seemingly appears to “speed up” in toroidal direction across the shock (i.e. $|v_{\text{LNRF}}^\phi(r)|$ increases across the shock) in LNRF although in radial direction the plasma indeed slows down (i.e. v_{CRF}^r decreases across the shock while hard to see in the plot) in CRF. This is explained as follows; we see $\Omega > 0$ and $\omega < 0$ at large radii in the upstream flow (i.e. $v_{\text{LNRF}}^\phi > 0$). Plasma is inevitably forced to slow down as it accretes due to frame-dragging and at some point it appears to come to a stop momentarily (i.e. $\Omega = 0$) with respect to the observer (i.e. still $v_{\text{LNRF}}^\phi > 0$). The plasma then turns around in the same sense as the BH rotation (i.e. still $\omega < \Omega < 0$ thus $v_{\text{LNRF}}^\phi > 0$ again) and later converges to the frame-dragging (i.e. $\Omega = \omega < 0$ thus $v_{\text{LNRF}}^\phi = 0$). Because of the initial angular momentum, the plasma subsequently “overshoots” in toroidal direction allowing for $\Omega < \omega < 0$ thus $v_{\text{LNRF}}^\phi < 0$. Past this phase, the plasma starts to converge to the BH rotation at small radii and eventually acquire $\Omega = \omega < 0$ thus $v_{\text{LNRF}}^\phi = 0$.

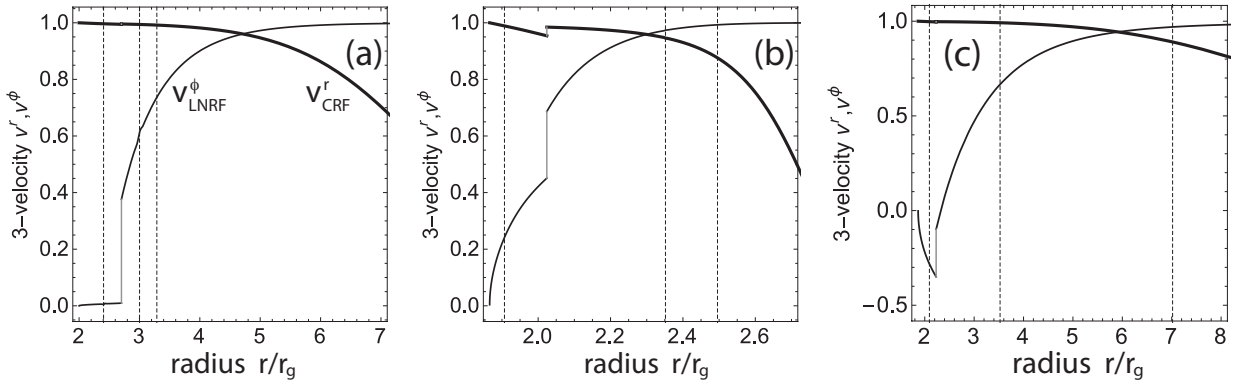


Fig. 3.— Same as Figure 2 but for physical three-velocity components v_{CRF}^r (thick) and v_{LNRF}^ϕ (solid) for accreting MHD plasma with (a) $a/M = 0$ (Schwarzschild BH), (b) 0.5 (prograde) and (c) -0.5 (retrograde).

Besides plasma kinematics, magnetization $\sigma(r)$ and plasma number density $n(r)$ are shown in Figure 4. Across the shock the upstream flow becomes compressed in all cases by definition causing the downstream flow to be heated where particles (primarily electrons) can be efficiently accelerated to later participate in Comptonization (see §3). Magnetization

parameter is initially negative at large radii because the Poynting flux in the upstream flow is directed radially outward while accretion energy flux always points inward. The Poynting flux is then shifted inward because B_ϕ switches its direction due to the curvature of the field line (see T02). In terms of energy budget of the plasma flow across fast MHD shocks, a fraction of upstream accretion energy is redistributed to both magnetic field and thermal energies and hence the magnetization always increases (via increasing B_ϕ) and entropy generation (via K) due to shock compression. The downstream region is therefore always more magnetized (i.e. $|\sigma_2| > |\sigma_1|$).

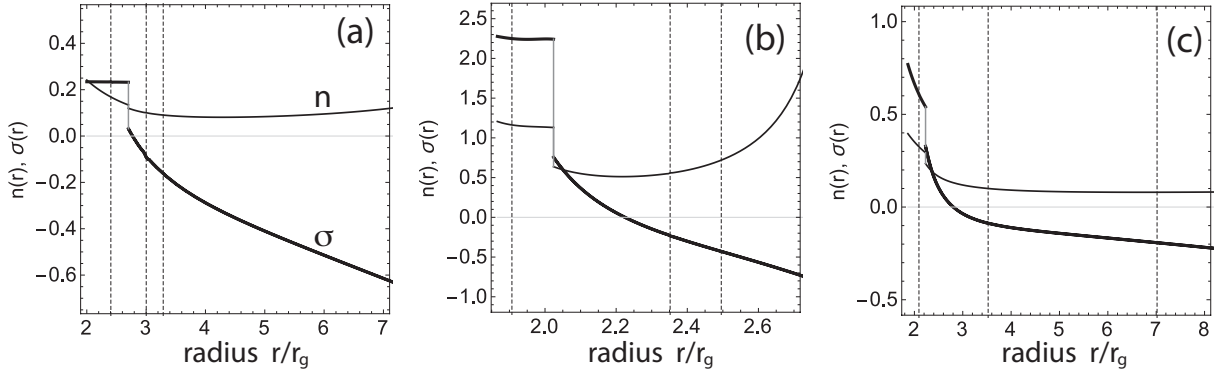


Fig. 4.— Same as Figure 2 but for plasma magnetization σ (thick) and number density n (solid) for accreting MHD plasma with (a) $a/M = 0$ (Schwarzschild BH), (b) 0.5 (prograde) and (c) -0.5 (retrograde).

Finally, we show in Figure 5 the downstream thermal energy $\Theta_e(r)$ of the trans-magnetosonic plasma as a function of normalized radius $x \equiv (r - r_H)/(r_{\text{sh}} - r_H)$ where r_{sh} is the shock location. As seen, the shock heating can raise the plasma thermal energy up to $\lesssim 40\%$ of the rest-mass energy of the plasma. It is found that $\Theta_e(r)$ only slowly varies with radius in almost all cases because (i) it is closely related to the density $n(r)$ which is almost constant in the postshock plasma (except for the retrograde case in (c)), (ii) the shock heating is not dissipated due to adiabatic assumption but advected and (iii) small radial size of the downstream flow. We will discuss later in §3 that the value of $\Theta_e(r)$ plays a fundamental role in determining the degree of Comptonization of incoming thermal disk photons.

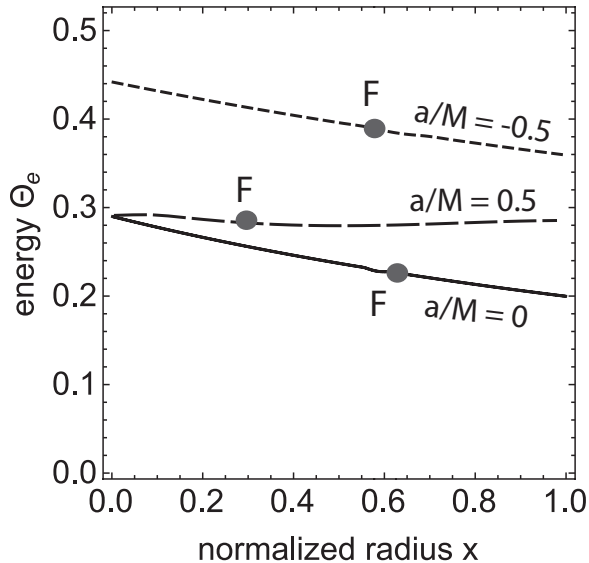


Fig. 5.— Same as Figure 2 but downstream electron energy $\Theta_e \equiv kT_e/(m_e c^2)$ for accreting plasma with $a/M = 0$ (solid), 0.5 (dotted) and -0.5 (dashed) where $x \equiv (r - r_H)/(r_{\text{sh}} - r_H)$ is a normalized radius between the horizon r_H and the shock location r_{sh} such that $x = 0$ at the horizon r_H while $x = 1$ at the shock location r_{sh} as defined in the text. A letter “F” denote the corresponding inner fast-point in each case.

3. Bulk Comptonization in the Hot Plasma

3.1. Comptonizing Process in the Downstream Plasma

Across a shock front electrons in accreting flow are efficiently compressed and heated up to sub-relativistic regime (i.e. $kT_e/m_e c^2 < 1$) in the postshock flow possibly via the first-order Fermi mechanism (e.g. Fermi 1949; Baring 1997; Gieseler & Jones 2000; Le & Becker 2005) in the presence of the randomly distributed, turbulent magnetic fields. Assuming that the energy due to shock heating $\Theta_e(r)$ is fully efficiently transported into particle (i.e. electrons) acceleration in the downstream flow with the energy of $(\gamma - 1)m_e c^2$, one can express the corresponding electron velocity ratio $\beta(\Theta_e)$ as

$$\beta(\Theta_e) \simeq \frac{\sqrt{\Theta_e(2 + \Theta_e)}}{1 + \Theta_e}, \quad (13)$$

via the usual Lorentz factor $\gamma \equiv (1 - \beta^2)^{-1/2}$. We consider that $\Theta_e(r)$ primarily characterizes the upper cut-off energy of the accelerated electron number distribution in the downstream

flow, i.e., $\beta_2(r) = \beta(\Theta_e)$, whereas the lower cut-off is arbitrarily assumed to be $\beta \equiv \beta_1 = 0.01$ in this work. Hence, shock heating can produce a nonthermal electron distribution in the downstream flow in the form of the power-law; i.e. the electron spectrum distribution is assumed to obey ϵ^q (e.g. Droege & Schlickeiser 1986) as speculated in the solar flares. In our work we assume a conservative slope of $q = -2$ (e.g. Zhong & Wang 2013) while the spectrum is only weakly sensitive to the exact value of q .

In the conventional view of the standard accretion disk scenario, disk surface radiates like blackbody of different temperature at a given point on the disk. The local intensity of disk blackbody between energy ϵ and $\epsilon + d\epsilon$ that is liberated at a point (r, ϕ) on the disk surface is given by Planck distribution

$$B_D(\epsilon, kT_{\text{in}})d\epsilon = \frac{8\pi\epsilon^2}{h^2c^2} \frac{1}{e^{\epsilon/kT_{\text{in}}} - 1} d\epsilon, \quad (14)$$

where ϵ is the thermal photon energy in a local disk frame and kT_{in} denotes the maximum disk temperature in the Shakura-Sunyaev model with GR correction as

$$kT_{\text{in}} \approx 10 \left(\frac{\dot{m}}{0.5}\right)^{1/4} \left(\frac{1}{m_8}\right)^{1/4} \left(\frac{r}{r_g}\right)^{-3/4} \left\{1 - \left(\frac{r_{\text{in}}}{r}\right)^{1/2}\right\}^{1/4} \text{ eV}, \quad (15)$$

emitted at the characteristic radius $r = r_D \equiv (49/6)r_g \approx 8r_g$ for $a/M = 0$ (e.g. Frank et al. 1992; Kato et al. 2008). While in reality the disk radiation is known to be multi-color spectrum (Mitsuda et al. 1984), in this work we assume that the hottest part of the disk predominantly contributes to a subsequent Comptonization. In other words, seed disk photons for Comptonization are assumed to originate primarily from $r = r_D$ where the disk temperature is maximum. Note, however, that both kT_{in} and r_D depend on the BH spin a . The disk continuum is then reprocessed by Compton up-scattering via energetic electrons in the hot downstream region with a shock front at $r = r_{\text{sh}} (< r_D)$ to produce the soft excess.

Following the same formalism by Zhong & Wang (2013), the differential Compton spectrum (i.e. Compton flux generated per solid angle per radius) in the local reference frame of downstream flow can be described as photon spectrum with $B_{\text{pl}}(\epsilon, kT_{\text{in}})$ being the blackbody intensity seen in the plasma frame; i.e. photon counts per time per area per energy is expressed as

$$I_{\text{Comp}}(\epsilon', kT_{\text{in}}) \propto \frac{1}{H_1(\beta_1, \beta_2)} \int_{\epsilon_o}^{\epsilon'} \frac{B_{\text{pl}}(\epsilon_{\text{pl}}, kT_{\text{in}})}{\epsilon_{\text{pl}}} H\left(\frac{\epsilon'}{\epsilon_{\text{pl}}}\right) d\epsilon_{\text{pl}}, \quad (16)$$

where ϵ_{pl} and ϵ' are respectively the incoming disk photon energy and the outgoing Comptonized photon energy measured in the rest-frame of the downstream plasma and

$$H\left(\frac{\epsilon'}{\epsilon}\right) = \begin{cases} \int_{\beta_1}^{\beta_2} (\gamma - 1)^{-q} \gamma^{-1} \beta^{-3} \zeta\left(\frac{\epsilon'}{\epsilon}, \beta\right) d\beta & \text{if } 1 \leq \frac{\epsilon'}{\epsilon} < \frac{1+\beta_1}{1-\beta_1}, \\ \int_{\beta_c}^{\beta_2} (\gamma - 1)^{-q} \gamma^{-1} \beta^{-3} \zeta\left(\frac{\epsilon'}{\epsilon}, \beta\right) d\beta & \text{if } \frac{1+\beta_1}{1-\beta_1} \leq \frac{\epsilon'}{\epsilon} \leq \frac{1+\beta_2}{1-\beta_2}, \\ 0 & \text{if } \frac{1+\beta_2}{1-\beta_2} < \frac{\epsilon'}{\epsilon}, \end{cases} \quad (17)$$

$$\zeta\left(\frac{\epsilon'}{\epsilon}, \beta\right) = \frac{\epsilon}{\epsilon'}(\beta+1)(\beta^2+1)\gamma^2 - \frac{\epsilon'}{\epsilon} \frac{1}{(\beta+1)\gamma^2} + 2 \left[\ln \left\{ \frac{\epsilon'}{\epsilon} \frac{1}{(\beta+1)^2\gamma^2} \right\} + \frac{\beta}{\beta+1} \right], \quad (18)$$

with a cut-off plasma velocity β_c defined as

$$\beta_c \equiv \frac{\epsilon'/\epsilon - 1}{\epsilon'/\epsilon + 1}, \quad (19)$$

and the lower integration limit ϵ_o is given by

$$\epsilon_o(\epsilon', \beta_2) = \epsilon' \left(\frac{1 - \beta_2}{1 + \beta_2} \right). \quad (20)$$

Lastly, the above coefficient $H_1(\beta_1, \beta_2)$ in equation (16) has been defined as

$$H_1(\beta_1, \beta_2) \equiv \int_{\beta_1}^{\beta_2} \gamma^5 \beta \left(1 + \frac{\beta^2}{3} \right) (\gamma - 1)^{-q} d\beta. \quad (21)$$

In addition, in terms of the photon energy, it is crucial to take into account the redshift factor of photons as they propagate from one point to the other under the curved spacetime because the Comptonizing region – hot downstream flow – is in a close proximity to the BH. Realizing that the postshock downstream region in this scenario typically lies within the ISCO (for both spinning and non-spinning BH cases) as depicted in Figure 1, disk photons are strongly subject to relativistic effects in several ways while they propagate from the disk surface at $r = r_D$ to the plasma downstream region at (r, ϕ) where $r_H \leq r \leq r_{sh} < r_D$ and $0 \leq \phi \leq 2\pi$; i.e. classical Doppler motion of the downstream plasma, special relativistic time dilation and gravitational redshift (e.g. Bardeen et al. 1972; Cunningham 1975; Kojima 1991; Hollywood & Melia 1997). The photon frequency is then shifted between the disk frame of the Keplerian motion and accreting plasma by factor of

$$g_1(r, \phi) \equiv \left| \frac{(p_\mu u^\mu)_{\text{pl}}}{(p_\mu u^\mu)_D} \right|_{\text{Disk} \rightarrow \text{Plasma}}, \quad (22)$$

where $p_\mu = (-E_{\text{ph}}, \pm E_{\text{ph}}(R(r))^{1/2}/\Delta, \pm(\Theta(\theta))^{1/2}, \xi E_{\text{ph}})$ denotes four-momentum of photons defined respectively in the plasma rest-frame (“pl”) and the disk rest-frame (“D”). In equation (22) above, note that we numerically solve null geodesic equations by GR ray-tracing (see §3.2) in radial $R(r)$ and angular $\Theta(\theta)$ directions with the photon energy E_{ph} in the emitted frame and its angular momentum component ξ (Chandrasekhar 1983, p.347). The disk blackbody intensity in equation (14) in the plasma downstream frame can then be expressed as

$$B_{\text{pl}}(\epsilon_{\text{pl}}, kT_{\text{in}}) = g_1^3 B_D(\epsilon_D, kT_{\text{in}}), \quad (23)$$

where $\epsilon_D \equiv \epsilon_{\text{pl}}/g_1$ is the seed photon energy in the disk frame using Lorentz invariance of photon intensity. Note that g_1 depends on (r, ϕ) because of relative motion between the Keplerian disk and accreting plasma. These photons are then locally Comptonized in all parts of the postshock flow as expressed in equations (16)-(21).

Assuming that the Comptonization takes place spatially uniformly within the downstream region ($r_H \leq r \leq r_{\text{sh}}$), the observed Comptonized intensity is given by

$$I_{\text{obs}}(\epsilon_{\text{obs}}, kT_{\text{in}}) \propto g_2(r, \phi)^3 I_{\text{Comp}}(\epsilon', kT_{\text{in}}) = g_2^3 I_{\text{Comp}}\left(\frac{\epsilon_{\text{obs}}}{g_2}, kT_{\text{in}}\right), \quad (24)$$

where

$$g_2(r, \phi) \equiv \left| \frac{(p_\mu u^\mu)_{\text{obs}}}{(p_\mu u^\mu)_{\text{pl}}} \right|_{\text{Plasma} \rightarrow \text{Observer}}. \quad (25)$$

provides the additional redshift factor of the reprocessed photon energy due to secondary relativistic effects with respect to a distant observer while those photons propagate under curved spacetime from the downstream plasma to the observer, as illustrated in Figure 1, such that $\epsilon' \equiv \epsilon_{\text{obs}}/g_2$. Therefore, the observed Comptonized intensity per radius is affected by the coupling between the two redshift effects, g_1 and g_2 , and found by

$$I_{\text{obs}}(\epsilon_{\text{obs}}, kT_{\text{in}}) \propto \frac{g_1(r, \phi)^3 g_2(r, \phi)^3}{H_1(\beta_1, \beta_2)} \int \frac{B_D(\epsilon_{\text{pl}}/g_1, kT_{\text{in}})}{\epsilon_{\text{pl}}} d\epsilon_{\text{pl}}, \quad (26)$$

Note, in equations (22) and (25), that different photon trajectories are considered and therefore g_1 is totally independent of g_2 . Thus, the corresponding differential flux via Comptonization is given by integrating over a solid angle subtended by the downstream region as

$$\frac{dF_{\text{obs}}}{dr} \propto \int \int_{\text{downstream}} I_{\text{obs}}(\epsilon_{\text{obs}}, kT_{\text{in}}) d\Omega_{\text{obs}}. \quad (27)$$

By further integrating over the downstream region in radius (i.e. $r_H \leq r \leq r_{\text{sh}}$) one can calculate the observed Comptonized spectrum

$$F_{\text{obs}} = \int_{r_H}^{r_{\text{sh}}} \left(\frac{dF_{\text{obs}}}{dr} \right) dr, \quad (28)$$

where $r_H \equiv [1 + (1 - a^2/M^2)^{1/2}]r_g$ is the radius of the event horizon normalized by the gravitational radius r_g and r_{sh} is the radius of the shock front in the accreting plasma. Lastly, the normalization of the model spectrum is currently treated as an independent parameter to be constrained by data (see §5).

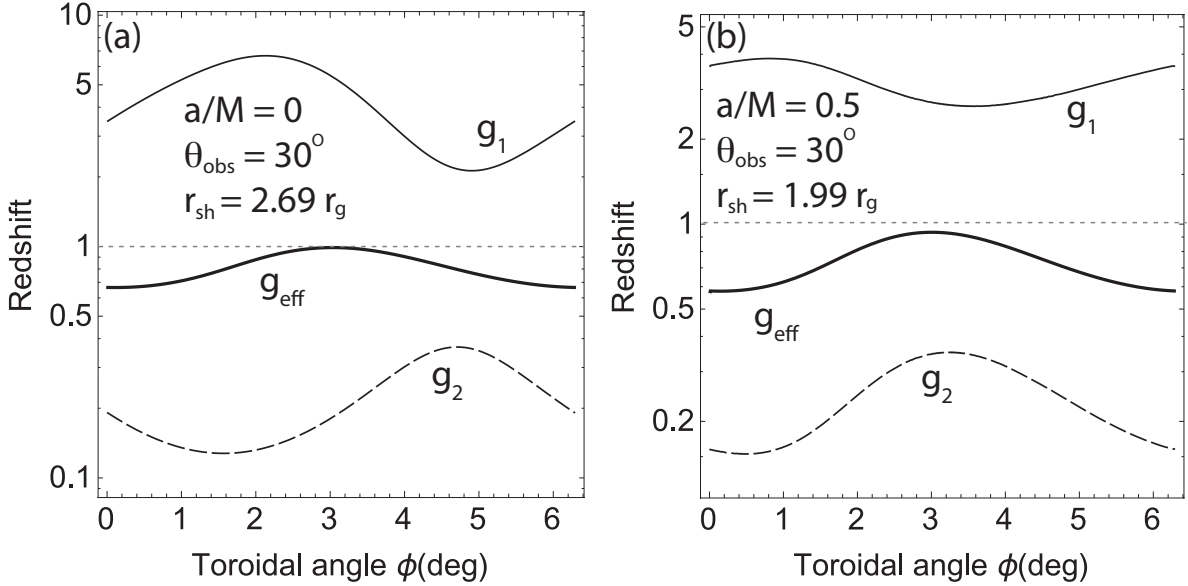


Fig. 6.— The transfer functions, $g_1(r_{\text{sh}}, \phi)$, $g_2(r_{\text{sh}}, \phi)$ and $g_{\text{eff}}(r_{\text{sh}}, \phi) \equiv g_1 \cdot g_2$, for the fiducial plasma accretion with (a) $a/M = 0$ and (b) 0.5 as a function of toroidal angle $0 \leq \phi \leq 2\pi$ at the shock location $r = r_{\text{sh}}$. See texts for the definitions and Table 1 for detailed parameters.

3.2. Transfer Functions with GR Ray-Tracing

Given a kinematic field of MHD accretion coupled with the conventional thermal disk radiation, one can calculate two redshift factors expressed in Eqns. (22) and (25). It is reminded that these factors are functions of radius and toroidal positions of plasma and the observed photon flux also depends on both g_1 and g_2 due to relativistic beaming. While incoming disk photons traveling towards the downstream plasma are always blueshifted ($g_1 > 1$), Comptonized photons from the plasma region are always redshifted ($g_2 < 1$) due to strong gravitational redshift being dominant over the longitudinal Doppler effect (at least for small angle $\theta \leq 45^\circ$ considered here). The transfer function (i.e. effective redshift factor), g_{eff} , is then the product of the two, $g_{\text{eff}} \equiv g_1 g_2$.

Employing the standard GR ray-tracing approach we calculate and store the transfer functions for different sets of inclination angle θ , BH spin a and the fiducial accretion solutions. As an example, Figure 6 shows g_1 , g_2 and g_{eff} as a function of azimuthal angle $0 \leq \phi \leq 2\pi$ at the shock location $r = r_{\text{sh}}$ for (a) $a/M = 0$ and (b) $a/M = 0.5$ assuming $\theta = 30^\circ$ with fiducial shocked plasma solutions similar to those in Table 1. With respect to the initial disk photon energy, the observed photons are found, as expected, to be always redshifted despite the blueshift from g_1 because the Comptonizing region (i.e. downstream

plasma) is sufficiently close to the horizon allowing for the factor g_2 to always dominate over the factor g_1 in redshift such that $0.5 \lesssim g_{\text{eff}} \lesssim 1.0$ as calculated. Note that the range of the effective redshift factor for both $a/M = 0$ and 0.5 appears to be very similar despite the spatial difference in the downstream plasma region; i.e. closer in towards the horizon for $a/M = 0.5$ case. This is due to a competition between g_1 and g_2 for a given BH spin. In other words, g_1 may be comparatively very large for $a/M = 0.5$ case because the downstream region is further closer in, while g_2 should then be correspondingly very small as Comptonized photons must climb up farther out towards the observer. As a result, a modest value of the effective redshift g_{eff} is always achieved almost regardless of the BH spin. These profiles are also found to be almost independent of radius $r_H \leq r \leq r_{\text{sh}}$ since the downstream region is very compact in radius. In §3.3 the computed transfer function is then used to calculate the Comptonized spectrum in combination with the MHD plasma solutions.

Table 2. Grid of `compsh` Model Parameters

| Primary Parameter | Value |
|--|--------------------------------|
| BH Spin a/m | $-0.5, 0, 0.5$ |
| Inclination Angle θ (degrees) | $15^\circ, 30^\circ, 45^\circ$ |
| Disk Temperature kT_{in} (eV) | 10, 20, 30, 40 |
| Downstream Elecetron Energy kT_e | See §3.3 |

3.3. Modeling Comptonized Spectra

Based on the numerical approach described in §3.1 and 3.2 we calculate the Comptonized spectra for various shocked plasma accretion with sets of fiducial disk blackbody temperature. Although in principle the effective disk temperature kT_{in} is strictly determined by the BH spin a , it is often speculated that the actual disk radiation is most likely subject to various scattering and reflection due to the (presumably corona-related) atmospheric property above the disk, which could slightly alter (if not substantially) the effective temperature of emerging thermal radiation (aka. color temperature) making the degree of color temperature index f_c be a sensitive quantity to assess the spectral property of the local thermal radiation. Following a number of previous works on disk color temperature (e.g. Ross et al. 1992; Shimura & Takahara 1995; Li et al. 2005; Davis et al. 2005; Done et al. 2012), we adopt the conventional value of $f_c = 1.7$ in this paper. Because of this uncertainty in estimating the exact disk temperature, in our calculations we introduce kT_{in} replacing the conventional kT_{in} and treated as a free parameter in the likelihood of the expected value (i.e. 10 – 40 eV) for a typical AGN disk environment. Among other independent model parameters, the primary ones to be intensively explored in this work include downstream electron energy⁴ kT_e , disk temperature kT_{in} and inclination angle θ_{obs} as listed in Table 2. Hence, the entire model spectrum in the present approach is characterized by these *three* quantities. By seeking a best-fit model, one can constrain the three parameters followed by the other important plasma quantities.

Figure 7a presents the calculated normalized spectra (in νF_ν) for different downstream electron energy kT_e assuming $kT_{\text{in}} = 30$ eV and $\theta_{\text{obs}} = 30^\circ$ for a given different BH spin. In each spin value, three spectra are computed with the lowest (solid), intermediate (dashed) and highest (dotted) shocked electron energy with $kT_{\text{in}} = 30$ eV and $\theta_{\text{obs}} = 30^\circ$; we select $kT_e = 33$ keV, 250 keV and 378 keV for $a/M = -0.5$ (gray); $kT_e = 75$ keV, 125 keV and 256 keV for $a/M = 0$ (solid); $kT_e = 126$ keV, 179 keV and 296 keV for $a/M = 0.5$ (thick). We stress here again that the energy kT_e is a dependent quantity determined by the shock location in the model for a given BH spin, thus not arbitrarily selected a priori. It is noted that the spectral peak can exceed ~ 1 keV depending on how much the downstream plasma is heated by the shock, and, as expected, they seem to be well correlated. The spectral shape is found to be more or less self-similar in a qualitative manner for different plasma flows and even BH spin values. This seems to be consistent with the observational fact that the detected soft excess can be almost uniquely accounted for in all AGNs with a single

⁴Downstream electron energy kT_e is actually a dependent parameter determined by a shock location r_{sh} for a given set of conserved plasma quantities. Nonetheless, we employ this variable in the current scheme to construct a library of model spectra later in §4.

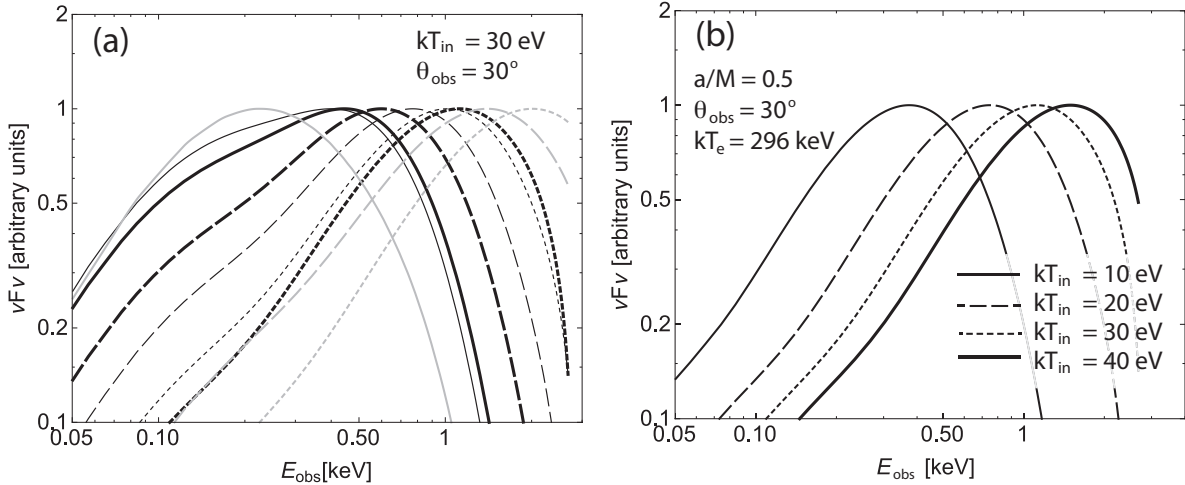


Fig. 7.— (a) Normalized Comptonized spectra νF_ν in the observer’s frame (without cosmological redshift) for various electron energy kT_e with $kT_{\text{in}} = 30$ eV and $\theta = 30^\circ$: $kT_e = 33$ keV, 250 keV and 378 keV for $a/M = -0.5$ (gray), 75 keV, 125 keV and 256 keV for $a/M = 0$ (dark), and 126 keV, 179 keV and 296 keV for $a/M = 0.5$ (thick solid). In each BH spin, temperature is lowest in *solid* curve, intermediate in *dashed* curve and highest in *dotted* one. (b) Normalized Comptonized spectra for various disk temperature with the fiducial accretion flow of $a/M = 0.5$, $kT_e = 296$ keV and $\theta_{\text{obs}} = 30^\circ$ (see Table 1): we show $kT_{\text{in}} = 10, 20, 30$ and 40 eV.

blackbody component of more or less the same temperature $kT \sim 0.1 - 0.2$ keV despite their potentially diverse circumnuclear conditions. Figure 7b shows a similar calculation but for different disk temperature kT_{in} with $a/M = 0.5$ and $\theta_{\text{obs}} = 30^\circ$: 10 eV (solid), 20 eV (dashed), 30 eV (dotted) and 40 eV (thick) for the same photon emitting radius r_D . It is clear that the peak energy of the emergent spectrum has a strong dependence on the disk temperature kT_{in} as expected. The expected Comptonized flux in this model is therefore strongly correlated with UV flux.

We also consider the effect of different inclination angle in Figure 8a for $\theta_{\text{obs}} = 15^\circ$ (solid), 30° (dashed) and 45° (dotted) assuming $a/M = 0$ and $kT_{\text{in}} = 30$ eV. We find that there is little change in the spectrum due to viewing angle. This is because the photon emitting region (i.e. downstream plasma) is generically (i) very close to the BH where gravitational redshift is predominant and (ii) the size of hot region is also very narrow in radius. Hence, in such proximity to the black hole the longitudinal Doppler blueshift

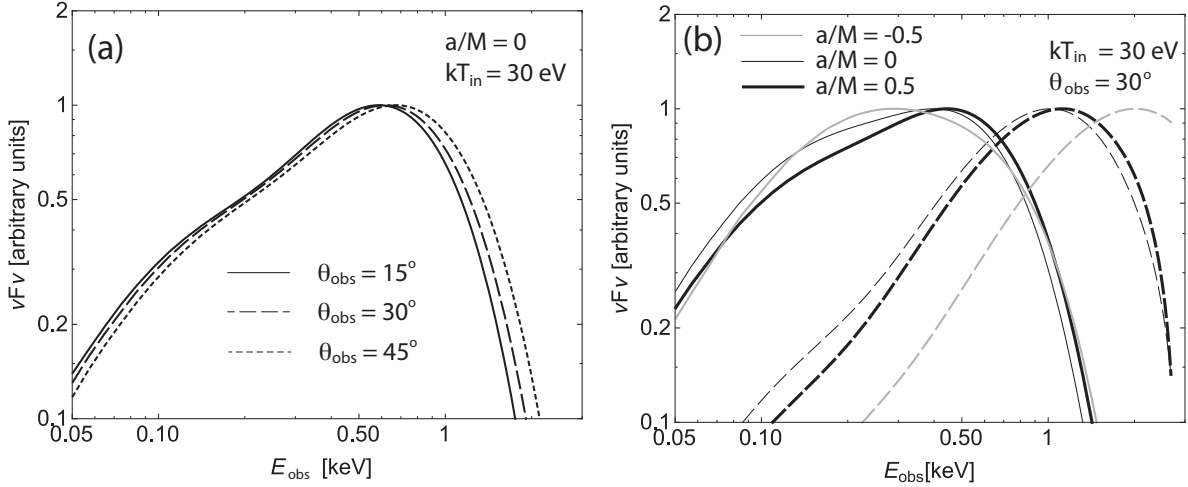


Fig. 8.— (a) Normalized Comptonized spectra for various inclination θ with $a/M = 0.5$, $kT_e = 179$ keV and $kT_{\text{in}} = 30$ eV (see Table 1): we show $\theta_{\text{obs}} = 15^\circ, 30^\circ$ and 45° . (b) Range of the normalized Comptonized spectra for various BH spin with $kT_{\text{in}} = 30$ eV and $\theta = 30^\circ$: solid/dashed curves are obtained from the lowest/highest electron energy considered for BH spin $a/M = -0.5$ (gray), 0 (dark) and 0.5 (thick solid).

never becomes significant enough to overcome the degree of gravitational redshift in all three cases. For this reason, this weak angle-dependence is seemingly very different from what one typically finds in the disk emission line, for example, broad iron fluorescence (e.g. Fabian et al. 1989; Kojima 1991). A spectral variation due to different BH spin a is examined in Figure 8b where $a/M = 0$ (dark), 0.5 (thick) and -0.5 (gray) for $kT_{\text{in}} = 30$ eV and $\theta_{\text{obs}} = 30^\circ$. Solid and dashed curve are obtained with the lowest and highest shocked electron energy in each BH spin, respectively.

As seen in this section, our calculations show that Comptonized disk photons in this scenario seem to be observationally plausible to account for the known soft excess feature in many Seyfert 1 X-ray spectra. To demonstrate its validity, we will apply this model in §4 to one of the well-known radio-quiet Seyfert 1 galaxy, Ark 120.

4. Case Study: Ark 120

Based on the model spectra for the soft excess component as shown in §3, we now apply the model to Ark 120, one of the well-studied luminous Seyfert 1 AGNs ($z = 0.0323$ and

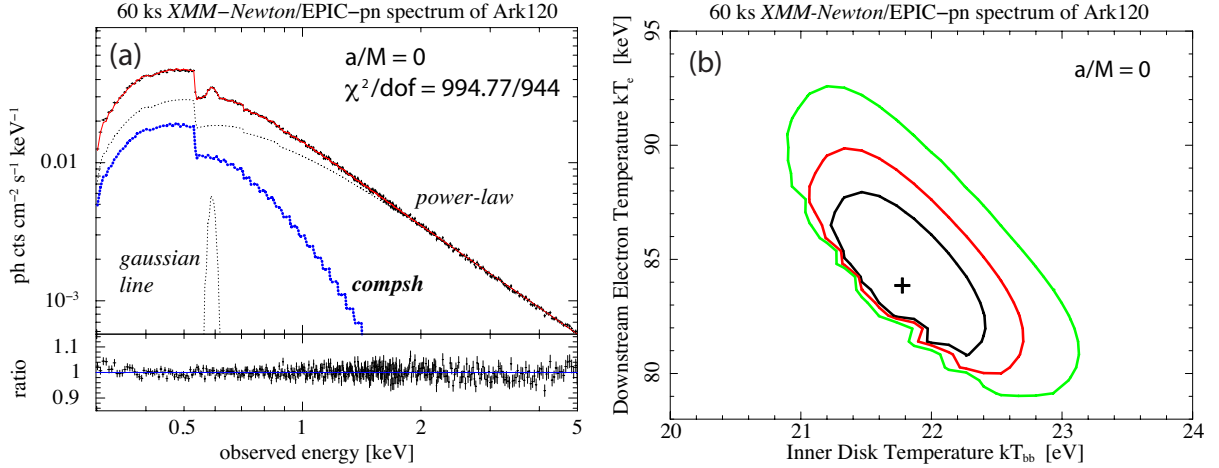


Fig. 9.— (a) 60ks *XMM-Newton*/EPIC-pn spectrum of Ark 120 fitted with the best-fit **compsh** model for a Schwarzschild BH of $a/M = 0$ and (b) its confidence contour plot showing 68%, 90%, and 99% regions relative to the best-fit model. See Table 3 for details.

$M \approx 2 \times 10^8 M_{\odot}$; e.g., Wandel et al. 1999; Peterson et al. 2004) in which little absorption features have been detected in both UV and X-ray bands despite the persistent presence of the soft excess (Turner & Pounds 1989; Brandt et al. 1993) which makes this particular AGN a “bare” nucleus (e.g. Vaughan et al. 2004).

As a case study to conclude the current work, we analyze a 60 ks *XMM-Newton*/EPIC-pn spectrum of Ark 120 observed in 2003 with the standard XSPEC 12.8.2 package (Arnaud 1996) to perform the χ^2 -statistics. All fit parameters are given in the source rest-frame ($z = 0.0323$) and errors are quoted at the 90% confidence level for one interesting parameter (i.e. $\Delta\chi^2 = 2.7$) unless otherwise stated. The Galactic column density, N_H , toward Ark 120 is fixed at $1.31 \times 10^{20} \text{ cm}^{-2}$ (Stark et al. 1992; Dickey & Lockman 1990). Throughout this paper, $H_o = 70 \text{ km s}^{-1} \text{ Mpc}^{-1}$ is assumed.

4.1. Best-fit compsh Model

By constructing a grid of Comptonized spectra spanned by the model parameters listed in Table 2, we develop a **compsh** model as an additive table model in XSPEC tool whose free parameters are (i) effective disk photon temperature kT_{in} [eV], (ii) downstream electron energy kT_e [keV], (iii) inclination angle θ_{obs} [deg] and (iv) corresponding normalization. Following the analysis by Vaughan et al. (2004) we freeze a single power-law of photon

index $\Gamma = 2$ to account for the continuum to the energy up to 5 keV. As previously reported (Vaughan et al. 2004; Matt et al. 2014), there has been indicative of an additional component at $E \gtrsim 7 - 8$ keV due presumably to disk (blurred) reflection as well as the well-defined iron emission line at ~ 6.4 keV. In this work we don't consider a putative reflection component since the proposed Comptonized model in this scenario is not directly (if not completely) related to those hard X-ray photon production⁵.

After applying the `compsh` model, we note a residual bump at ~ 0.55 keV which can be attributed to the instrumental and Galactic oxygen edges (Vaughan et al. 2004). We independently treat this feature with a single gaussian line (`zga`) as performed in Vaughan et al. (2004). Thus, our composite model is symbolically expressed as `phabs*(po+atable{compsh}+zga)` where `po` is the power-law continuum and `phabs` denotes the Galactic absorption. As stated in §3.3, the `compsh` spectrum model is determined only by the above *three* primary parameters besides its normalization; i.e. kT_{in} , kT_e and θ_{obs} and independent of the other spectral components at least explicitly.

We present our results for $a/M = 0$ (Fig. 9), $a/M = 0.5$ (Fig. 10) and $a/M = -0.5$ (Fig. 11) where a 60-ks *XMM-Newton*/EPIC-pn data is fitted with the `compsh` model in each case. First, the soft excess is found to be successfully accounted for by the proposed model yielding an excellent statistical significance in which the derived best-fit parameters are well constrained as shown in the contour plots at 68%, 90% and 99% level as shown.

The derived values of the best-fit parameters of the proposed models are listed in Table 3 for each case including the characteristic radii for plasma flows as well as the standing shock properties. Note that these radii derived in the table are not free-parameters but dependent variables. We first note that all three cases are equally well constrained yielding a reasonable χ^2 values for all three cases. With the seed disk photons of characteristic temperature ($\lesssim 20 - 30$ eV), the best-fit downstream energy kT_e tends to increase with the BH spin primarily because the shock location tends to slightly shift inward bringing the downstream region inward with the spin. The Comptonized spectra for $a/M = 0.5$ are therefore subject to a more drastic gravitational redshift in the observer's frame requiring the downstream electron temperature kT_e to be higher in the plasma rest-frame (before being redshifted) to balance. The derived viewing angle θ_{obs} seems to be systematically low to intermediate for three cases consistent with the conventional classification scheme of the Seyfert galaxies such as Ark 120. Note also in Table 3 that the characteristic magnetosonic radii and the Alfvén radius are all closer together in the case of $a/M = 0.5$. The shock

⁵While reflection may be remotely related to disk photons via coronae, emitting regions in this scenario are physically very distant from each other and thus such a weak correlation, if any, would be smeared out.

compression (i.e. shock strength), n_2/n_1 , is well correlated with the electron energy kT_e as compression is the source of generating additional entropy in the downstream flow. Since we are focusing in this work on fast MHD shocks, the field line becomes more refracted away from the shock normal (i.e. away from radial direction) across the shock front (i.e. $|B_{\phi,2}| > |B_{\phi,1}|$), the dissipated plasma energy is partially transformed to the field energy consistent with increasing magnetization parameter $\sigma_2 > \sigma_1$ as shown in Table 3. The rate of increase in magnetization σ due to shock is also well correlated with the BH spin (see, e.g., T02). Among the three BH spins, for $a/M = 0$ and 0.5 cases, the derived disk temperature is statistically consistent ($kT_{\text{in}} \approx 21 - 23$ eV) within the uncertainty. On the other hand, it appears that the retrograde BH spin of $a/M = -0.5$ is slightly more favored by observations indicating a relatively higher disk temperature $kT_{\text{in}} = 34.0$ eV and a slightly lower electron energy $kT_e = 61.3$ keV in comparison with the other two cases as seen in Table 3. One way to understand this result is the following; in the retrograde case, incoming disk photons are emitted primarily at a larger disk radius according to equation (15) while the downstream region remains to be formed at small radii (i.e. $r_{\text{sh}}/r_g = 2.16$). Thus, the emitted photons from the disk are subject to more blueshift in the rest-frame of the downstream plasma. For such Comptonized photons with more blueshift, high electron energy kT_e would not be necessary to counteract against a subsequent gravitational redshift while propagating towards the observer. Whereas even lower electron energy $kT_e (\lesssim 61\text{keV})$ for $a/M = -0.5$ can be statistically viable as shown in Figure 11b, we find that no plasma accretion in this case is allowed to develop a downstream region that is “colder” than $kT_e \sim 61$ keV as seen in Figure 11b which is contrasted with the other two cases where the confidence level is unambiguously constrained as shown in Figures 9b and 10b.

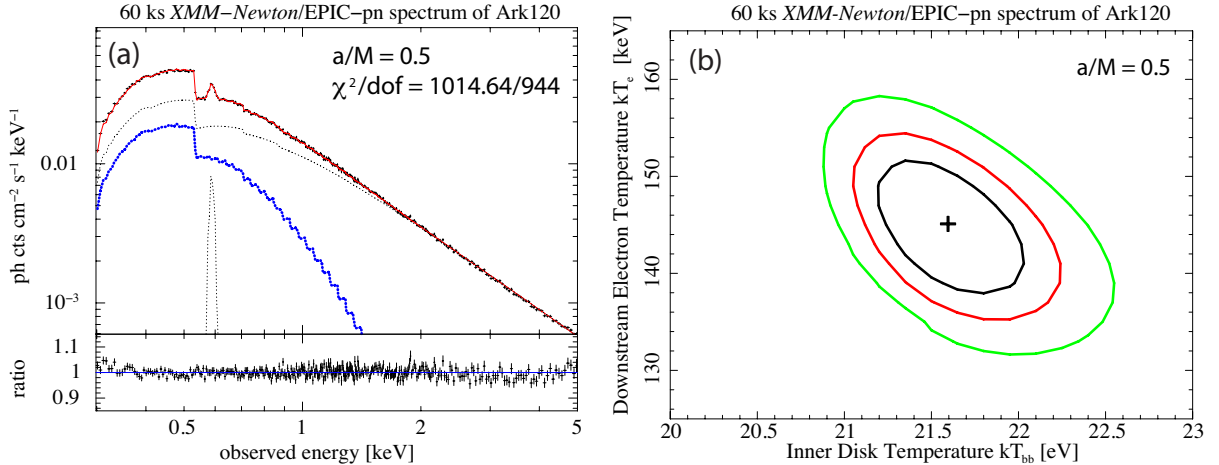


Fig. 10.— (a) Same as Figure 9 but for $a/M = 0.5$ (prograde).

Table 3. Best-fit GRMHD compsh Models[†]

| Parameter | Description | BH Spin a/M | | |
|---------------------------|----------------------------|-----------------------|--------------------------|--------------------------|
| | | -0.5 | 0 | 0.5 |
| kT_e [keV] [†] | Electron Energy | $61.3_b^{+2.0}$ | $83.5_{-2.8}^{+4.2}$ | $144.3_{-6.8}^{+7.2}$ |
| kT_{in} [eV] | Disk Temperature | $34.0_{-10.3}^{+1.3}$ | $21.7_{-0.53}^{+0.64}$ | $21.6_{-0.40}^{+0.46}$ |
| θ_{obs} [deg] | Inclination Angle | $17.5_{-1.4}^{+5.2}$ | $42.6_{-7.3}^a$ | $36.6_{-3.5}^{+4.3}$ |
| r_A/r_g | Alfvén Point | $8.27_{-0.028}^a$ | $3.28_{-0.001}^{+0.002}$ | $2.48_{-0.001}^{+0.001}$ |
| r_F^{out}/r_g | Outer Fast Point | 3.53 ± 0.0001 | 3.00 ± 0.0001 | 2.35 ± 0.0001 |
| r_{sh}/r_g | Shock Location | $2.16_b^{+0.004}$ | $2.69_{-0.001}^{+0.002}$ | $1.99_{-0.004}^{+0.005}$ |
| r_F^{in}/r_g | Inner Fast Point | $2.11_{-0.0003}^a$ | $2.42_{-0.003}^{+0.002}$ | $1.90_{-0.001}^{+0.001}$ |
| n_2/n_1 | Compression Ratio | $1.08_b^{+0.008}$ | $1.10_{-0.001}^{+0.002}$ | $1.82_{-0.008}^{+0.01}$ |
| σ_1 | Upstream Magnetization | $0.41_{-0.006}^a$ | $0.037_{-0.001}^{0.001}$ | $1.07_{-0.05}^{+0.06}$ |
| σ_2 | Downstream Magnetization | $0.49_{-0.0005}^a$ | $0.21_{-0.002}^{+0.004}$ | $2.82_{-0.11}^{+0.12}$ |
| $B_{\phi 2}/B_{\phi 1}$ | Toroidal Field Enhancement | $1.11_b^{+0.014}$ | $5.01_{-0.17}^{+0.25}$ | $1.43_{-0.021}^{+0.025}$ |
| χ^2/dof | | 961.91/944 | 994.77/944 | 1014.64/944 |

All radii are normalized to the gravitational radius r_g .

[†] Assuming that $M_8 = 1, q = -2, \beta_1 = 0.01$ and $f_c = 1.7$.

^a Upper parameter value reached.

^b Lower parameter value reached.

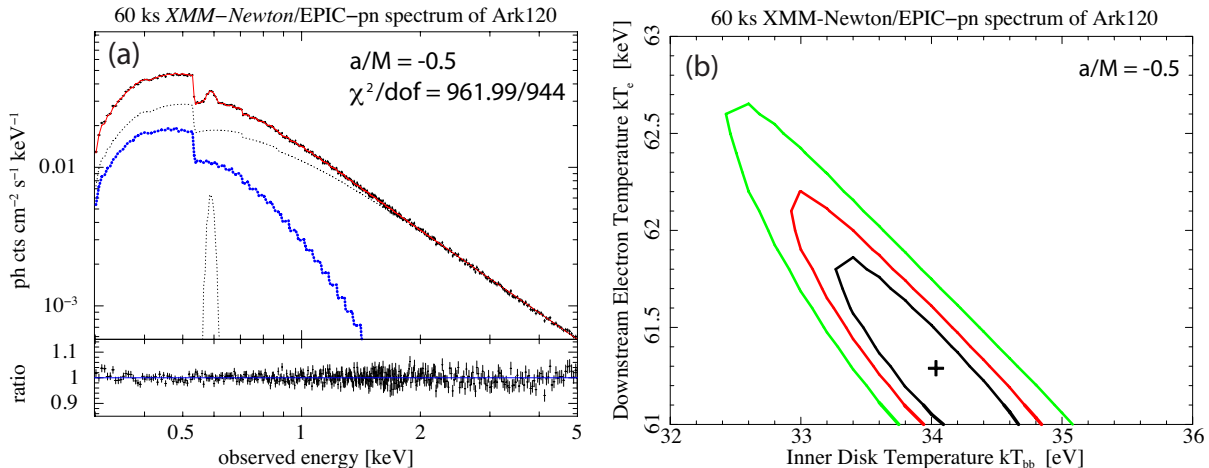


Fig. 11.— (a) Same as Figure 9 but for $a/M = -0.5$ (retrograde).

5. Summary & Conclusion

In this work we proposed a novel scenario that a shock-heated downstream flow in GRMHD accretion, injected from near the ISCO, serves as an ideal heating site where accelerated electrons can Compton up-scatter thermal disk photons to imprint the observed soft excess component in the AGN X-ray spectrum. Extending our earlier work on GRMHD standing shock formation, we explored sets of fiducial solutions for accreting plasma in Kerr geometry and studied their physical conditions in terms of liberated energy via shocks. Given a monochromatic blackbody radiation originating from the hottest part of the disk, we calculated Comptonized spectra by making use of the obtained plasma accretion. Our calculations are all fully relativistic including photon redshift among the disk rest-frame, plasma rest-frame and the distant observer’s rest-frame by employing GR ray-tracing approach. As a simplistic three-parameter model (i.e. θ_{obs} , kT_e and kT_{in}) besides its normalization, we have constructed a grid of synthetic spectral model for Comptonized component (`compsh`) and further demonstrated that the model can successfully explain the observed soft excess feature for a typical Seyfert 1 galaxy, Ark 120, as a case study.

We show that GRMHD plasma in this model begins to plunge in from radii very close to the ISCO within the standard disk paradigm. It is found that the downstream region, heated by fast MHD shocks, typically extends out to only a few gravitational radii. While we only consider equatorial accretion for simplicity, plasma in reality is expected to accrete along a closed-loop of poloidal field lines within the ISCO developing shocks as shown in F07 where the vertical height of the shock is systematically found to be $h \lesssim 5r_g$ for various accretion parameters. Such a very compact and centrally-concentrated region resembles a long-sought physical identity of the putative X-ray “coronal” region near the BH that

is inevitably required for explaining the basis of the major spectral components in AGN X-ray observations (e.g. Haardt & Maraschi 1991; Miniutti et al. 2003; Petrucci et al. 2004; Nardini et al. 2011; Fabian et al. 2015; Keck et al. 2015; Lohfink et al. 2015). For example, Kara et al. (2015) has analyzed the broad-band X-ray spectrum of a narrow-line Seyfert galaxy, 1H0707-495, to estimate a very compact coronal source at the height of $h \sim 2r_g$ above a rapidly-rotating BH in the context of the standard lamp-post model, while its physical identification of the X-ray source in that extreme proximity is yet to be confirmed theoretically. Our GRMHD calculations indicate that the formation of such a “corona” is ubiquitous and almost universal for a wide range of plasma parameter space including BH spin and the χ^2 analysis successfully derived the range of $61.3 \text{ keV} \lesssim kT_e \lesssim 144.3 \text{ keV}$, $21.6 \text{ eV} \lesssim kT_{\text{in}} \lesssim 34.0 \text{ eV}$ and $17.5^\circ \lesssim \theta_{\text{obs}} \lesssim 42.6^\circ$, although the model slightly favors the retrograde BH case ($a/M = -0.5$) as shown in Table 3. While a discussion of physical arrangement of such a retrograde AGN system is beyond the scope of this paper, counterrotating plasma (with respect to BH rotation) allows for a larger Comptonizing area due to a larger ISCO radius (e.g. Chandrasekhar 1983; Bardeen et al. 1972; Cunningham 1975). Hence, the resulting composite spectrum from the downstream flow can afford to produce a more diverse spectral shape when integrating over the downstream region. This may be the reason why the soft excess in data seems to be better accounted for by a retrograde BH case. The current model, however, does not provide a fundamental explanation of such a retrograde BH spin and it is only empirical in this framework. A retrograde BH, allowing for the disk to recede further out, may also be viable with the fact that Ark 120 seems to exhibit no strong signs for absorption (thus a “bare” nucleus) which would otherwise be expected to be present in soft X-ray band. We note, however, that the earlier studies of Ark 120 seem to imply a somewhat intermediate BH spin of $a/M \sim 0.5 - 0.6$ based on the ionized reflection models while with some potential uncertainties (e.g. García et al. 2014; Matt et al. 2014).

In the present work we have only considered moderate BH spin values ($-0.5 \leq a/M \leq 0.5$) because we found it rather challenging to systematically obtain the solutions for very high BH spin values ($a/M \gtrsim 0.9$) as the size of the downstream region becomes even more compact in radius. A more thorough parameter search will be a future work.

In comparison with a recent thermal Comptonization scenario proposed by Petrucci et al. (2013) for MrK 509, the Comptonizing “corona” (i.e. $60 \lesssim kT_e \lesssim 150 \text{ keV}$ within the ISCO) in our model is very similar to “hot corona” (e.g. $kT_{\text{hc}} \sim 100 \text{ keV}$ at the innermost region of accretion responsible for the power-law component) but different from “warm corona” ($kT_{\text{wc}} \sim 0.6 \text{ keV}$ exterior to the hot corona responsible for the soft excess) in their model in terms of its geometry and physical characteristics (see their Fig. 10). A critical difference between the two models lies in the fact that the spectral distribution of Comptonizing particles (i.e. electrons) is assumed to be nonthermal (i.e. power-law) as described in §3.1. while Petrucci et al. (2013) considers thermal distribution. Although our

current model focuses only on the production of soft excess through shocks, it is very likely that a local magnetic field activity on the disk surface such as reconnection might play a major role in producing nonthermal continuum in hard X-ray regime.

As has been widely debated to date in the literature, relativistically-blurred reflection model may also be able to explain the observed excess feature (e.g. Ponti et al. 2010; De Marco et al. 2013; Lohfink et al. 2012; Vasudevan et al. 2014; Crummy et al. 2006) while expecting a strong spectral correlation between the soft and hard X-rays due to their direct coupling in production process. In the framework of our current model, on the other hand, the production site of the soft excess component is strictly confined to the innermost plasma accretion set by the shock formation within the ISCO radius and thus physically disentangled from reflected hard X-rays expecting no correlation between the two. In recent studies of broad-band spectroscopies from a number of Seyfert galaxies showing the strong soft excess, however, we note that detailed spectral analyses seem to disfavor such an expected correlation but indicate a correlation between UV and soft X-ray flux (e.g. Mehdipour et al. 2011; Petrucci et al. 2013; Boissay et al. 2014, 2015). Our model, by definition, is co-aligned with the latter findings. While not definitive yet, our scenario is consistent with those findings at least qualitatively. As discussed by Matt et al. (2014), on the other hand, the actual correlation could be rudimentary as the soft excess could be present without a pronounced relativistic reflection component, and it takes more effort to draw a conclusion.

It is found that Comptonization due to standing shock is very sensitive to the shock property controlled primarily by the downstream energy kT_e while not so significantly dependent on BH spin a in that the calculated spectra are almost generically self-similar regardless of the exact value of BH spin. This may thus be indicative of model degeneracy with BH spin. In the present calculations we treat arbitrarily the normalization of Comptonized spectrum as a free parameter. That is, the flux level of the calculated excess component is not determined by the model but is only provided by data. Technically speaking, the intensity of the excess component must be coupled with plasma property (such as density, temperature and magnetic field strength) and should be self-consistently calculated by the model. It is important, however, to examine how much energy is physically available in the postshock region in comparison with the observed soft excess flux. To clearly address the modeled excess intensity, a more rigorous consideration of the `compsh` normalization is necessary as a future work. While still open to debate how much Comptonized flux can be produced from the small downstream region, one might argue that relativistic beaming (via light bending effect) of seed photons towards small radii could preferentially allow for a sufficient centrally-concentrated illumination (e.g. Fukumura & Kazanas 2007a). This may yield enough Comptonized photons possibly in a scenario analogous to the observed double-peaked $H\alpha$ emission line from AGN accretion disk (e.g. Chen et al. 1989; Eracleous & Halpern 1994; Strateva et al. 2008).

In this work, we assumed a split-monopole field configuration. Although not globally applicable, this is an approximate solution to the trans-field equation (i.e. GR GS-equation) as originally discussed in Blandford & Znajek (1977). Interestingly, state-of-the-art numerical simulations in recent years from different groups indicate a characteristic field topology very similar to that described as the split-monopole (Hirose et al. 2004; Tchekhovskoy, McKinney, & Narayan 2009; Contopoulos, Kazanas, & Papadopoulos 2013). Although a detailed structure and strength of the actual magnetic field at the horizon scale still remains unclear, this approximation is a first step forward to the problem. Nonetheless, the accreting plasma models listed in Table 1 yield the field strength on the order of $B \sim 10^{3-4}$ G consistent with the known estimates to date (e.g. Krolik 1999; Wang et al. 2001; Fukumura et al. 2007).

While treated as fully relativistic under strong gravity, we note that the current model is time-independent based on axisymmetric plasma. This assumption makes it impossible for us to predict any temporal nature of the soft excess considered in this work; e.g. spectral time variabilities associated with shock compression and cooling effects. The downstream plasma properties are numerically solved by considering adiabatic (nonradiative) Rankine-Hugoniot jump conditions as a pure mathematical discontinuity with no energy/mass loss. Hence, most of the heat generated at the shock front is advected with the downstream plasma. A more realistic shock process, on the other hand, is most likely accompanied by radiative cooling to some degree in which the postshock plasma temperature may stay comparatively as cool as that of the upstream one as in the isothermal shocks (e.g. Lu & Yuan 1998; Das et al. 2003; Fukumura et al. 2004; Fukumura & Kazanas 2007b). Radiative dissipation at the shock front could therefore drastically change the subsequent downstream plasma condition which in turn alters the Comptonization process. In reality, furthermore, accreting plasma may be characterized by a two-temperature gas between electrons and ions (e.g. Shapiro et al. 1976; Mahadevan 1998; Manmoto 2000) unless the Coulomb coupling between the two is very efficient, whereas in this work we prescribed a single-fluid approximation for simplicity. Becker et al. (2011) have considered a particle transport process (e.g. bulk advection, spatial diffusion and particle escape) via the effects of the first-order Fermi acceleration across a standing shock. In a more self-consistent scenario such a calculation of diffusive shock acceleration should be incorporated to reflect the energetic outflows/jets from the shock front. Although all these micro-physics should be addressed and incorporated into more sophisticated calculations by GRMHD simulations for completeness, this is beyond the scope of this paper.

The other potentially important spectral components associated with magnetic fields include synchrotron radiation, and its Comptonization have also been extensively considered in the literature in the context of black hole binaries such as Cygnus X-1, for example, via nonthermal powerlaw electrons (e.g. Wardziński & Zdziarski 2001; Chakrabarti & Mandal 2006). While this is especially important in black hole binaries, the characteristic

synchrotron frequency in AGNs is estimated to be $\nu_{\text{syn}} \simeq 4 \times 10^{10} B_4 \gamma_e^2$ [Hz] $\sim 1.6 \times 10^{-4}$ [eV] where B_4 is the field strength in units of 10^4 G and we take $\gamma_e \sim 1$ in this model. Hence, those Comptonized photons are less likely to be significant to the composite spectrum from the innermost accretion region of AGNs that are considered in this work.

We have analyzed in this work a Seyfert galaxy, Ark 120, to demonstrate that the proposed model successfully describes the observed soft excess feature within the framework of a simplistic accretion model. As there is a number of archival X-ray data available mainly from typical narrow-line Seyfert AGNs and PG quasars that also exhibit strong excess components (e.g. Crummy et al. 2006, for 20 to 30 AGNs) in the *XMM-Newton*/EPIC-pn observations, we will extend the current study to those available for a more systematic analysis. Despite a simplistic prescription of the proposed scenario based on GRMHD shock formation, our Comptonization model is successful in describing the observed soft excess feature in Ark 120. We thus find the current result to be an encouraging first step towards the next level where additional relevant physics are employed to make the model more physically self-consistent and promising.

As a next-generation X-ray observatory, we anticipate advanced new X-ray missions, such as *Athena*, to contribute significantly to this study particularly with the high-resolution X-ray microcalorimeter spectrometer by providing more detailed spectra simultaneously on the soft and hard X-ray components. The expected data will thus help differentiate various (fundamentally) distinct models presented today and further clarify the current ambiguous views concerning the observed soft excess in the immediate circumnuclear region of AGNs.

The authors acknowledge the anonymous referee for useful comments and questions. KF is grateful to Omer Blaes for his insightful suggestions about the disk simulations and Rozenn Boissay for a number of useful comments. A part of this work was conducted while at KITP of UCSB and also supported in part by the 4-VA Collaborative at James Madison University.

REFERENCES

- Acharya, K., Chakrabarti, S. K. & Molteni, D. 2002, JApA, 23, 155
- Armitage, P. J., Reynolds, C. S., & Chiang, J. 2001, ApJ, 548, 868
- Arnaud, K. A. 1996, in ASP Conf. Ser. 101, Astronomical Data Analysis Software and Systems V, ed. G. H. Jacoby & J. Barnes (San Francisco, CA: ASP), 17
- Bardeen, J. M., Press, W. H., & Teukolsky, S. A. 1972, ApJ, 178, 347
- Baring, M. G. 1997, in Very High Energy Phenomena in the Universe, ed. Y. Giraud-Heraud & J. Tran Thanh Vanastro (Paris: Editions Frontières), 97
- Becker, P. A., Das, S. & Le, T. 2011, ApJ, 743, 47
- Boissay, R., Paltani, S., Ponti, G., Bianchi, S., Cappi, M., Kaastra, J. S., Petrucci, P.-O., Arav, N., Branduardi-Raymont, G., Costantini, E., Ebrero, J., Kriss, G. A., Mehdipour, M., Pinto, C. & Steenbrugge, K. C. 2014, A&A, 567, 44
- Boissay, R., Paltani, S. & Ricci, C. 2015, The Extremes of Black Hole Accretion, Proceedings of the conference
- Boller, T., Brandt, W. N., & Fink, H. 1996, A&A, 305, 53
- Blandford, R. D., & Znajek, R. L. 1977, MNRAS, 179, 433
- Brandt, W. N., Fabian, A. C., Nandra, K., & Tsuruta, S. 1993, MNRAS, 265, 996
- Chakrabarti, S. K. 1990, Theory of Transonic Astrophysical Flows (Singapore: World Scientific)
- Chakrabarti, S. K. 1995, Seventeenth Texas Symposium on Relativistic Astrophysics and Cosmology, Annuals of the New York Academy of Sciences, Vol. 759 (New York, NY: The New York Academy of Sciences), p.546
- Chakrabarti, S. & Titarchuk, L. G. 1995, ApJ, 455, 623
- Chakrabarti, S. K. & Mandal, S. 2006, ApJ, 642, L49
- Chandrasekhar, S. 1983, The Mathematical Theory of Black Holes (Oxford: Oxford Univ. Press)
- Chen, K., Halpern, J. P. & Filippenko, A. V. 1989, ApJ, 339, 742
- Contopoulos, I., Kazanas, D., & Papadopoulos, D. B. 2013, ApJ, 765, 113

- Crummy J., Fabian A.C., Gallo L., & Ross R.R. 2006, MNRAS, 365, 1067
- Cunningham, C. T. 1975, ApJ, 202, 788
- Das, T. K., Pendharkar, J. K. & Mitra, S. 2003, ApJ, 592, 1078
- Das, S. & Chakrabarti, S. K. 2007, MNRAS, 374, 729
- Davis, S. W., Blaes, O. M., Hubeny, I., & Turner, N. J. 2005, ApJ, 621, 372
- De Marco, B., Ponti, G., Cappi, M., Dadina, M., Uttley, P., Cackett, E. M., Fabian, A. C., & Miniutti, G. 2013, MNRAS, 431, 2441
- Dickey, J. M. & Lockman, F. J. 1990, ARA&A, 28, 215
- Di Gesu, L., CostanMni, E., Piconcelli, E., et al. 2014, A&A, 563, A95
- Done, C., Davis, S. W., Jin, C., Blaes, O., & Ward, M. 2012, MNRAS, 420, 1848
- Droege, W. & Schlickeiser, R. 1986, ApJ, 305, 909
- Eracleous, M. & Halpern, J. P. 1994, ApJS, 90, 1
- Fabian, A. C., Rees, M. J., Stella, L., & White, N. E. 1989, MNRAS, 238, 729
- Fabian, A. C., Miniutti, G., Gallo, L., Boller, Th., Tanaka, Y., Vaughan, S. & Ross, R. R. 2004, MNRAS, 353, 1071
- Fabian, A. C., Zoghbi, A., Ross, R. R., et al. 2009, Nature, 459, 540
- Fabian, A. C., Lohfink, A., Kara, E., Parker, M. L., Vasudevan, R., & Reynolds, C. S. 2015, MNRAS, 451, 4375
- Fermi, E. 1949, Phys. Rev., 75, 1169
- Fragile, P. C., Blaes, O. M., Anninos, P., & Salmonson, J. D. 2007, ApJ, 668, 417
- Fragile, P. C. & Blaes, O. M. 2008, ApJ, 687, 757
- Frank, J., King, A., & Raine, D. 1992, *Accretion Power in Astrophysics* (2nd ed.; Cambridge: Cambridge Univ. Press)
- Fukumura, K. & Tsuruta, S. 2004, ApJ, 611, 964
- Fukumura, K., Takahashi, M. & Tsuruta, S. 2007, ApJ, 657, 415 (F07)
- Fukumura, K. & Kazanas, D. 2007a, ApJ, 664, 14

- Fukumura, K. & Kazanas, D. 2007b, *ApJ*, 669, 85
- García, J., Dauser, T., Lohfink, A., Kallman, T. R., Steiner, J. F., McClintock, J. E., Brenneman, L., Wilms, J., Eikmann, W., Reynolds, C. S. & Tombesi, F. 2014, *ApJ*, 782, 76
- Generozov, A., Blaes, O., Fragile, P. C., & Henisey, K. B. 2014, *ApJ*, 780, 81
- Gierliński, M. & Done, C. 2004, *MNRAS*, 349, 7
- Gieseler, U. D. J., & Jones, T. W. 2000, *A&A*, 357, 1133
- Goodrich, R. W. 1989, *ApJ*, 342, 224
- Haardt, F., & Maraschi, L. 1991, *ApJ*, 380, L51
- Hirose, S., Krolik, J. H., De Villiers, J.-P. & Hawley, J. F. 2004, *ApJ*, 606, 1083
- Hollywood, J. M. & Melia, F. 1997, *ApJS*, 112, 324
- Kara, E., Fabian, A. C., et al. 2015, *MNRAS*, 449, 234
- Kato, S., Fukue, J., & Mineshige, S. 2008, *Black Hole Accretion Disks* (2nd ed.; Kyoto: Kyoto Univ. Press)
- Keck, M. L. et al. 2015, *ApJ*, 806, 149
- Koide, Shinji; Shibata, Kazunari; Kudoh, Takahiro, 1998, *ApJ*, 495, 63
- Koide, Shinji; Meier, David L.; Shibata, Kazunari; Kudoh, Takahiro, 2000, *ApJ*, 536, 668
- Krolik, J. H. 1999, *Active Galactic Nuclei* (Princeton: Princeton Univ. Press)
- Leighly, K. M. 1999a, *ApJS*, 125, 297
- Leighly, K. M. 1999b, *ApJS*, 125, 317
- Kojima, Y. 1991, *MNRAS*, 250, 629
- Laor, A., Fiore, F., Elvis, M., Wilkes, B. J., & McDowell, J. C. 1997, *ApJ*, 477, 93
- Le, T. & Becker, P. A. 2005, *ApJ*, 632, 476
- Li, L.-X., Zimmerman, E. R., Narayan, R., & McClintock, J. E. 2005, *ApJS*, 157, 335
- Lohfink, A. M., Reynolds, C. S., Miller, J. M., Brenneman, L. W., Mushotzky, R. F., Nowak, M. A. & Fabian, A. C. 2012, *ApJ*, 758, 67

- Lohfink, A. M., et al. 2015, *ApJ*, 814, 24
- Lu, J.-F., Yu, K. N., Yuan, F., & Young, E. C. M. 1997, *A&A*, 321, 665
- Lu, J.-F. & Yuan, F. 1998, *MNRAS*, 295, 66
- Mahadevan, R. 1998, *Nature*, 394, 651
- Manmoto, T. 2000, *ApJ*, 534, 734
- Matt, G., et al. 2014, *MNRAS*, 439, 3016
- Mehdipour, M., Branduardi-Raymont, G., Kaastra, J. S., Petrucci, P. O., Kriss, G. A., Ponti, G., Blustin, A. J., Paltani, S., Cappi, M., Detmers, R. G., & Steenbrugge, K. C. 2011, *A&A*, 534, 39
- Michel, F. C. 1973, *ApJ*, 180, L133
- Middleton, M., Done, C. & Gierliński, M. 2007, *MNRAS*, 381, 1426
- Mineshige, S., Kawaguchi, T., Takeuchi, M. & Hayashida, K. 2000, *PASJ*, 52, 499
- Miniutti, G., Fabian, A. C., Goyder, R., & Lasenby, A. N. 2003, *MNRAS*, 344, L22
- Miniutti, G. & Fabian, A. C. 2004, *MNRAS*, 349, 1435
- Mitsuda, K., Inoue, H., Koyama, K., Makishima, K., Matsuoka, M., Ogawara, Y., Suzuki, K., Tanaka, Y., Shibazaki, N., & Hirano, T. 1984, *PASJ*, 36, 741
- Molteni, D., Sponholz, H., Chakrabarti, S. K. 1996, *ApJ*, 457, 805
- Molteni, D., Gerardi, G., Valenza, M. A. & Lanzafame, G. 1999, *Observational Evidence for the Black Holes in the Universe*, Conference held in Calcutta, January 11-17th, p.83
- Morales T. D., Fragile, P. C., Zhuravlev, V. V., & Ivanov, P. B. 2014, *ApJ*, 796, 103
- Nagakura, H. & Yamada, S. 2008, *ApJ*, 689, 391
- Nardini, E., Fabian, A. C., Reis, R. C., & Walton, D. J. 2011, *MNRAS*, 410, 1251
- Nobuta, K. & Hanawa, T. 1994, *PASJ*, 46, 257
- Noda, H., Makishima, K., Nakazawa, K., Uchiyama, H., Yamada, S., & Sakurai, S. 2013, *PASJ*, 65, 4
- Okuda, T., Teresi, V., Toscano, E., & Molteni, D. 2004, *PASJ*, 56, 547
- Okuda, Y., Teresi, V. & Molteni, D. 2007, *MNRAS*, 377, 1431

- Osterbrock, D. E. & Pogge, R. W. 1985, *ApJ*, 297, 166
- Peterson, B. M., Ferrarese, L., Gilbert, K. M., Kaspi, S., Malkan, M. A., Maoz, D., Merritt, D., Netzer, H., Onken, C. A., Pogge, R. W., Vestergaard, M., & Wandel, A. 2004, *ApJ*, 613, 682
- Petrucci, P. O., Maraschi, L., Haardt, F. & Nandra, K. 2004, *A&A*, 413, 477
- Petrucci, P.-O., Paltani, S., Malzac, J., et al. 2013, *A&A*, 549, A73
- Ponti, G., Gallo, L. C., Fabian, A. C., Miniutti, G., Zoghbi, A., Uttley, P., Ross, R. R., Vasudevan, R. V., Tanaka, Y. & Brandt, W. N. 2010, *MNRAS*, 406, 2591
- Pu, H.-Y., Nakamura, M., Hirovani, K., Mizuno, Y., Wu, K. & Asada, K. 2015, *ApJ*, 801, 56
- Ross, R. R., Fabian, A. C. & Mineshige, S. 1992, *MNRAS*, 258, 189
- Ross R.R. & Fabian A.C. 2005, *MNRAS*, 358, 211
- Schurch, N. J. & Done, C. 2006, *MNRAS*, 371, 81
- Schurch, N. J. & Done, C. 2008, *MNRAS*, 386, 1
- Shakura, N. I.; Sunyaev, R. A. 1973, *A&A*, 24, 337
- Shapiro, S. L., Lightman, A. P., & Eardley, D. M. 1976, *ApJ*, 204, 187
- Shimura, T. & Takahara, F. 1995, *ApJ*, 445, 780
- Stark, Antony A., Gammie, C. F., Wilson, R. W., Bally, J., Linke, R. A., Heiles, C., & Hurwitz, M. 1992, *ApJS*, 79, 77
- Strateva, I. V., Brandt, W. N., Eracleous, M. & Garmire, G. 2008, *ApJ*, 687, 869
- Takahashi, M., Rilett, D., Fukumura, K. & Tsuruta, S. 2002, *ApJ*, 572, 950 (T02)
- Takahashi, M., Goto, J., Fukumura, K., Rilett, D. & Tsuruta, S. 2006, *ApJ*, 645, 1408 (T06)
- Takahashi, M. & Takahashi, R. 2010, *ApJ*, 714, 176
- Tchekhovskoy, A., McKinney, J. C. & Narayan, R. 2009, *ApJ*, 699, 1789
- Tchekhovskoy, A., Narayan, R. & McKinney, J. C. 2011, *MNRAS*, 418, 79
- Titarchuk, L., Mastichiadis, A. & Kylafis, N. D. 1996, *A&AS*, 120, 171

- Turner, T. J. & Pounds, K. A. 1989, MNRAS, 240, 833
- Vasudevan, R. V., Mushotzky, R. F., Reynolds, C. S., Fabian, A. C., Lohfink, A. M., Zoghbi, A., Gallo, L. C. & Walton, D. 2014, ApJ, 785, 30
- Vaughan, S., Fabian, A. C., Ballantyne, D. R., De Rosa, A., Piro, L., & Matt, G. 2004, MNRAS, 351, 193
- Wald, R. M. 1974, Phys. Rev. D, 10, 1680
- Walter, R. & Fink, H. H. 1993, A&A, 274, 105
- Wandel, A.; Peterson, B. M.; Malkan, M. A. 1999, ApJ, 526, 579
- Wang, T. G., Matsuoka, M., Kubo, H., Mihara, T., & Negoro, H. 2001, ApJ, 554, 233
- Wardziński, G. & Zdziarski, A. A. 2001, MNRAS, 325, 963
- Wilkins, D. R., Gallo, L. C., Grupe, D., Bonson, K., Komossa, S. & Fabian, A. C. 2015, MNRAS, 454, 4440
- Zhong, X. & Wang, J. 2013, ApJ, 773, 23